The Astrophysical Journal, 598:785–803, 2003 December 1

DUST IN THE EARLY UNIVERSE: DUST FORMATION IN THE EJECTA OF POPULATION III SUPERNOVAE

Takaya Nozawa and Takashi Kozasa
Division of Earth and Planetary Sciences, Graduate School of Science, Hokkaido University, Sapporo 060-0810, Japan;
nozawa@ep.sci.hokudai.ac.jp, kozasa@ep.sci.hokudai.ac.jp

and

Hideyuki Umeda, Keiichi Maeda, and Ken'ichi Nomoto
Department of Astronomy, School of Science, University of Tokyo, Bunkyo-ku, Tokyo 113-0033, Japan;
umeda@astron.s.u-tokyo.ac.jp, maeda@astron.s.u-tokyo.ac.jp, nomoto@astron.s.u-tokyo.ac.jp
Received 2003 June 28; accepted 2003 August 11

ABSTRACT

Dust grains play a crucial role in the formation and evolution history of stars and galaxies in the early universe. We investigate the formation of dust grains in the ejecta of Population III supernovae, including pair-instability supernovae, which are expected to occur in the early universe, applying a theory of non–steady state nucleation and grain growth. Dust formation calculations are performed for core-collapse supernovae with progenitor mass $M_{\rm pr}$ ranging from 13 to 30 $M_\odot$ and for pair-instability supernovae with $M_{\rm pr} = 170$ and 200 $M_\odot$. In the calculations, the time evolution of gas temperature in the ejecta, which strongly affects the number density and size of newly formed grains, is calculated by solving the radiative transfer equation, taking account of the energy deposition of radioactive elements. Two extreme cases are considered for the elemental composition in the ejecta, unmixed and uniformly mixed cases within the He core, and formation of CO and SiO molecules is assumed to be complete. The results of calculations for core-collapse supernovae and pair-instability supernovae are summarized as follows: in the unmixed ejecta, a variety of grain species condense, reflecting the difference of the elemental composition at the formation site in the ejecta; otherwise only oxide grains condense in the uniformly mixed ejecta. The average size of newly formed grains spans a range of 3 orders of magnitude, depending on the grain species and the formation condition, and the maximum radius is limited to less than 1 μm, which does not depend on the progenitor mass. The size distribution function of each grain species is approximately lognormal, except for Mg silicates, MgO, Si, and FeS in the unmixed case and Al_2O_3 in both cases. The size distribution function summed up over all grain species is approximated by a power-law formula whose index is -3.5 for the larger radius and -2.5 for the smaller one; the radius at the crossover point ranges from 0.004 to 0.1 μm, depending on the model of supernovae. The fraction of mass locked into dust grains increases with increasing the progenitor mass: 2%–5% of the progenitor mass for core-collapse supernovae and 15%–30% for pair-instability supernovae whose progenitor mass ranges from 140 to 260 $M_\odot$. Thus, if very massive stars populated the first generation of stars (Population III stars), a large amount of dust grains would be produced in the early universe. We also discuss the dependence of the explosion energy and the amount of ^{56}Ni in the ejecta, as well as the efficiency of formation of CO and SiO molecules, on the formation of dust grains in the ejecta of supernovae.

Subject headings: dust, extinction — early universe — supernovae: general
On-line material: color figures

1. INTRODUCTION

The recent observations of the reddening of background quasars and the damped Lyα systems in the spectra of distant quasars have confirmed the presence of dust grains in the high-redshift universe (e.g., Pettini et al. 1994, 1997; Pei & Fall 1995). Dust grains play a critical role in the formation and evolution history of stars and galaxies in the early universe: dust grains absorb stellar light and reemit it by thermal radiation, which controls the energy balance in interstellar space and the evolution of gas clouds. Also, the surface of dust grains is an efficient site for the formation of H_2 molecules, which act as an effective coolant at the time of the formation of stars from interstellar clouds, enhance the star formation rate (SFR), and strongly affect the initial mass function (IMF) in the metal-poor universe (Hirashita, Hunt, & Ferrara 2002; Hirashita & Ferrara 2002). In fact, the most iron-poor star so far discovered, HE 0107−5240 (Christlieb et al. 2002), has raised important questions about the formation of such a metal-poor ([Fe/H] = -5.3 ± 0.2) but low-mass ($\sim$0.8 $M_\odot$) star. Umeda & Nomoto (2003a) showed that this star can be the second-generation star formed from a gas cloud enriched by a Population III supernova that produced very little Fe but enough C and O for efficient gas cooling. Schneider et al. (2003b) also considered this star as the second generation but argued that the dust grains produced by Population III objects could play an important role in forming low-mass stars from a gas cloud as metal-poor as metallicity $Z = 10^{-5.1} Z_\odot$. Furthermore, dust grains residing in interstellar space in galaxies and in the intergalactic medium cause obscuration and reddening of starlight, and the thermal radiation from the dust grains distorts the cosmic background radiation (see Hauser & Dwek 2001 for details).

How much dust grains absorb stellar light and reemit it by thermal radiation heavily depends on their chemical composition, size, and abundance. Therefore, the investigation of dust grains in the early universe is inevitable not only to reveal the structure and evolution of the early universe, but also to deduce the SFR and the IMF during the evolution of the universe from the observations of the cosmic microwave background (CMB) and the cosmic infrared background (CIB), which could be one of the main subjects of the planned Atacama Large Millimeter Array (ALMA) and the *James Webb Space Telescope* (*JWST*, formerly the *Next-Generation Space Telescope*; Loeb & Haiman 1997).

In cosmic environments, dust grains form in a cooling gas outflowing from star to interstellar space, such as in the stellar winds from asymptotic giant branch (AGB) stars and in the ejecta of supernovae. The major source of dust grains in our Galaxy is considered to be AGB stars evolving from stars with a main-sequence mass of $\leq 8\ M_{\odot}$. However, the age of AGB stars is too old to contribute to dust grains in the early universe. Thus, supernovae evolving from stars whose main-sequence mass is larger than $8\ M_{\odot}$ are considered to be the major source of dust grains in the early universe. Dust formation in the ejecta of supernovae has been suggested from the isotopic anomalies in meteorites, and the microscopic analysis of dust grains extracted from meteorites has identified SiC, graphite, and Si_3N_4 grains as the supernovae condensates (SUNOCONs) from their isotopic composition (see Zinner 1998 for details). SN 1987A is the first supernova in which the in situ dust formation in the expanding ejecta was observed (Lucy et al. 1989; Whitelock et al. 1989; Meikle et al. 1993; Wooden et al. 1993; Colgan et al. 1994), and the model of formation of dust grains in the ejecta was investigated by Kozasa, Hasegawa, & Nomoto (1989a, 1989b, 1991). Also, dust formation was confirmed in the ejecta of SN 1999em from the appearance of blue-shifted line emissions, as observed in SN 1987A (Elmhamdi et al. 2003).

What kind of and how many dust grains condense in the ejecta are still in debate. The observations of young supernova remnants (SNRs) with the *Infrared Space Observatory* (*ISO*) revealed the thermal radiation from dust grains condensed in the ejecta of Cas A (Lagage et al. 1996; Arendt, Dwek, & Moseley 1999), and the observed thermal radiation is well fitted by a mixture of Al_2O_3, $MgSiO_3$, and SiO_2 grains (Douvion, Lagage, & Pantin 2001b); however, the spectroscopic observations at 2.4–45 μm suggested that the pristine dust in Cas A is a peculiar class of silicate material (Arendt et al. 1999). On the other hand, no thermal radiation originating from dust grains formed in the ejecta was observed toward the Tycho, Kepler, and Crab SNRs by *ISO* (Douvion et al. 2001a), despite the fact that the optical observations have suggested the presence of dust grains in the Crab SNR (Fesen & Blair 1990; Hester et al. 1990). The estimated amount of hot dust observed in the Cas A SNR by *ISO* (Arendt et al. 1999) is 10–100 times smaller than the value previously estimated from *IRAS* observations (e.g., Mezger et al. 1986; Dwek et al. 1987). However, the recent submillimeter observations by SCUBA have revealed the existence of cold dust in the young SNR of Cas A, leading to the conclusion that the amount of dust condensed in the ejecta is estimated to reach a few solar masses (Dunne et al. 2003). These observations strongly support the hypothesis that Type II supernovae could be the major source of dust grains in the early universe.

Of course, the chemical composition, size, and amount of dust grains in the early universe are determined by the balance between production in the ejecta of supernovae and destruction by interstellar shock, as well as reverse shock penetrating into the ejecta (see, e.g., Dwek 1998 for details), and the investigation of dust formation in the ejecta of Population III supernovae is the first step to revealing the nature of dust grains in the early universe. Todini & Ferrara (2001) performed dust formation calculations in primordial core-collapse supernovae (CCSNe) with progenitor mass $M_{\rm pr}$ ranging from 12 to 35 $M_{\odot}$, adopting the models of supernovae by Woosley & Weaver (1995) and applying the method of dust formation calculation for SN 1987A by Kozasa et al. (1989a, 1991) as a template. In the calculations, they considered a one-zone model for elemental composition and density in the ejecta, assuming the uniform mixing of elements within the He core. Taking account of the formation and destruction of CO and SiO molecules, they showed that carbon grains condense first and that Al_2O_3, Mg silicates, and Fe_3O_4 grains then condense in this order as the gas cools down. Also, they showed that the size of newly formed grains is relatively small ($\leq$300 Å in radius) and is sensitive to the value of adiabatic index γ and that the total mass of dust produced is about 0.08–0.3 $M_{\odot}$ per supernova.

The recent theoretical investigations of fragmentation of gas clouds in the metal-free early universe have claimed that stars more massive than some tens to 100 $M_{\odot}$ populate the first generation (Nakamura & Umemura 2001; Bromm, Coppi, & Larson 2002). Such metal-free stars as massive as $140\ M_{\odot} \leq M_{\rm pr} \leq 260\ M_{\odot}$ may evolve stably to end their lives as pair-instability supernovae (PISNe; e.g., Umeda & Nomoto 2002; Heger & Woosley 2002). Also Umeda & Nomoto (2002) have suggested that hypernovae (HNe), whose explosion energy is more than several to 10 times that of ordinary CCSNe, are necessary to reproduce the enhancement of Zn and iron-peak elements observed in metal-poor stars. Therefore, in this paper, we explore dust formation in the ejecta of Population III supernovae, including HNe and PISNe, to investigate the dependence of the progenitor mass and the explosion energy on the formation of dust grains in the ejecta. Our main aim is to clarify the dependence of the yield of newly formed grains and their size on the progenitor mass, focusing on the ordinary CCSNe and PISNe. We also investigate the effects of the explosion energy and the mass of ^{56}Ni in the ejecta, as well as the efficiency of formation of CO and SiO molecules, on the formation of dust grains.

As discussed by Kozasa et al. (1989a), the elemental composition in the ejecta controls what kind of grain species condenses, and the temporal evolution of gas density and temperature in the ejecta strongly affects the size of newly formed grains in the ejecta. Thus, in the dust formation calculations we employ the hydrodynamic models and elemental compositions of Population III supernovae calculated by Umeda & Nomoto (2002). The time evolution of gas temperature is calculated by the multifrequency radiative transfer code, taking account of the energy deposition from radioactive elements (Iwamoto et al. 2000). Two extreme cases for the elemental composition in the ejecta are considered: the original onion-like structure (hereafter referred to as the unmixed case) and the uniformly mixed case within the He core. A theory of non–steady state nucleation and grain growth is applied for the calculation of dust formation, under the assumption that the formation of CO

and SiO molecules is complete. The formation of all possible condensates is taken into account simultaneously, to clarify what kind of grain species really condenses.

In § 2 we present the models of supernovae used in the calculations, and the method of dust formation calculation is described in § 3. The results of calculations for ordinary CCSNe and PISNe are presented and discussed in § 4 and summarized in § 5. The effects of the explosion energy and the amount of ^{56}Ni in the ejecta, as well as the efficiency of formation of CO and SiO molecules, on dust formation in the ejecta of supernovae are presented in Appendices A and B, respectively.

2. MODEL OF THE POPULATION III SUPERNOVAE

The nature of Population III supernovae has been extensively investigated to decipher the chemical evolution of the early universe compared with the observed elemental abundance of metal-poor stars (Umeda & Nomoto 2002, 2003b). Umeda & Nomoto (2002) have suggested that, in addition to ordinary CCSNe with explosion energies of $\sim 10^{51}$ ergs, HNe, whose explosion energies are larger than $(5\text{–}50) \times 10^{51}$ ergs (e.g., Nomoto et al. 2001, 2003 for reviews), are necessary to reproduce the enhancement of Zn and iron-peak elements observed in metal-poor stars. Also, in the metal-free universe very massive stars, with mass ranging from 140 to 260 $M_\odot$, evolve stably and explode as PISNe, in which a star is completely disrupted by a nuclear-powered explosion (Umeda & Nomoto 2002; Heger & Woosley 2002).

We apply the hydrodynamic models and the results of nucleosynthesis calculations of Population III supernovae by Umeda & Nomoto (2002) for the dust formation calculations. The details of the models used in the present calculations are summarized in Table 1, where the labels C, P, and H in the model names represent ordinary CCSNe, PISNe, and HNe, respectively, and the numerical value denotes the mass of the progenitor in units of solar mass. The mass cut is the mass coordinate of the boundary between the ejecta and the remnant, and its value specifies the mass of ^{56}Ni in the ejecta; $M(^{56}\mathrm{Ni}) = 0.07\ M_\odot$ is taken as a typical value for ordinary CCSNe to reproduce the observed behavior of the early light curve. The models of HNe (H20A, H20B, H30A, and H30B) are adopted to investigate the dependence of the explosion energy and the mass of ^{56}Ni in the ejecta on dust formation. The elemental composition and temporal evolution of gas density and temperature in the ejecta, which are essential to investigating dust formation, are summarized in the following subsections.

2.1. *Elemental Composition*

The elemental composition in the ejecta determines what kind of grain species condenses. No dust grain condenses in the hydrogen envelope of Population III supernovae, because the hydrogen envelope is metal-free. Even if heavy elements intrude into the hydrogen envelope during the evolution of the progenitor, the low density and the high expansion velocity prevent dust grains from condensing in the hydrogen envelope, as discussed by Kozasa et al. (1989a, 1991). Thus, the dust formation region in the ejecta of Population III supernovae is confined within the He core, where heavy elements exist.

Figure 1 shows the elemental composition within the unmixed He core at day 600 after the explosion, taking account of the decay of radioactive elements. Figure 1*a* is for a model of CCSNe (C20) and Figure 1*b* for PISNe (P170). The ejecta is divided into five regimes, according to the elemental composition of interest to dust formation: for example, in the ejecta of model C20, an Fe-Si-S layer ($2.45\ M_\odot \le M_r \le 2.52\ M_\odot$), a Si-S-Fe layer ($2.52\ M_\odot \le M_r \le 2.95\ M_\odot$), an O-Si-Mg layer ($2.95\ M_\odot \le M_r \le 3.14\ M_\odot$), an O-Mg-Si layer ($3.14\ M_\odot \le M_r \le 4.92\ M_\odot$), and a He layer ($4.92\ M_\odot \le M_r \le 5.79\ M_\odot$).

The He layer is carbon-rich (C/O > 1) for CCSNe, and its mass irregularly varies with the progenitor mass in the models of CCSNe used in this paper. The mass of the oxygen-rich layer (the O-Si-Mg and O-Mg-Si layers) increases with increasing progenitor mass, and the mass of the inner Si-S-Fe and Fe-Si-S layers depends on the value of the mass cut. On the other hand, in the ejecta of PISNe, the He layer is very thin for model P170, and the mass increases with increasing progenitor mass.

The mixing of elements in the ejecta of SN 1987A was confirmed from the early emergence of X-rays and γ-rays (e.g., Dotani et al. 1987; Itoh et al. 1987; Kumagai et al. 1988), and also hydrodynamic simulations (Hachisu et al. 1990; see Arnett et al. 1989 for a review and references) and laboratory experiments (Drake et al. 2002) clearly demonstrate that the mixing of elements is caused by the Rayleigh-Taylor instability at each interface of layers with different

TABLE 1
MODELS OF SUPERNOVAE USED IN THE CALCULATIONS

Model	Progenitor Mass ($M_\odot$)	Explosion Energy E_{51} (10^{51} ergs)	Mass Cut ($M_\odot/M_r$)	He Core Mass ($M_\odot$)	$M(^{56}\mathrm{Ni})$ ($M_\odot$)
C13	13	1	1.50	2.05	0.07
C20	20	1	2.45	5.79	0.07
C25	25	1	2.54	8.01	0.07
C30	30	1	2.54	10.7	0.07
P170	170	20	0	82.4	3.56
P200	200	28	0	117.3	7.25
H25A	25	10	3.29	8.01	0.07
H25B	25	10	2.47	8.01	0.7
H30A	30	30	5.31	10.9	0.07
H30B	30	30	4.33	10.9	0.7

NOTE.—In the model names, the labels C, P, and H represent ordinary CCSNe, PISNe, and HNe, respectively, and the numerical value denotes the mass of the progenitor in units of solar mass.

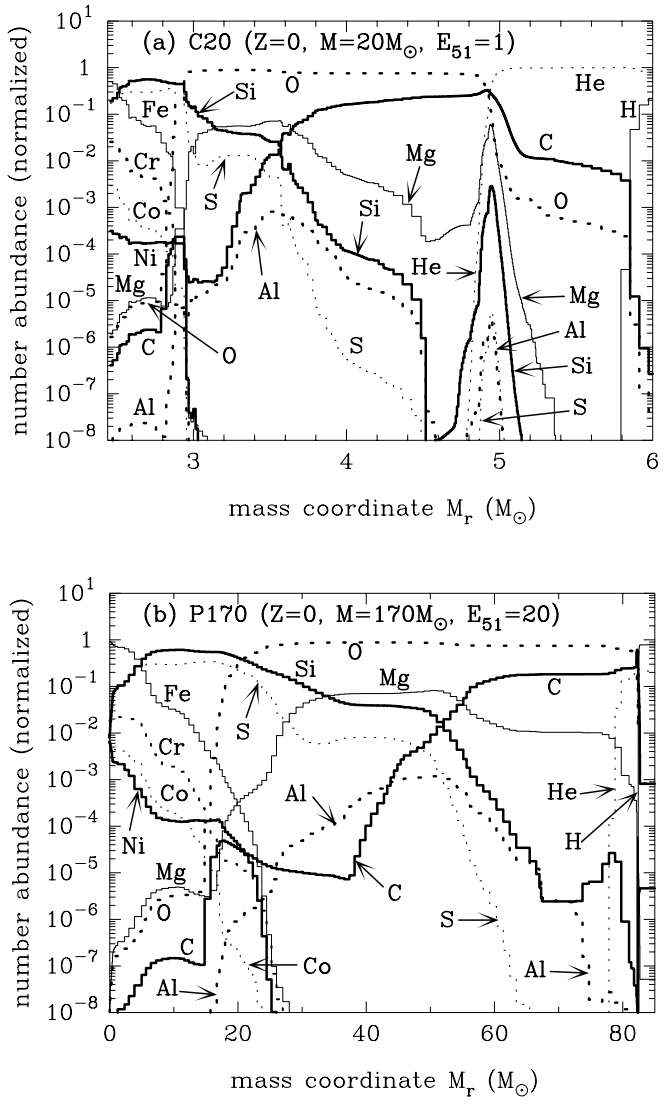

FIG. 1.—Number abundance of elements relevant to dust formation within the unmixed He core at 600 days after the explosion, taking into account the decay of radioactive elements, for (*a*) C20 and (*b*) P170. [*See the electronic edition of the Journal for a color version of this figure.*]

elemental compositions. The isotopic signatures in the presolar carbon and SiC grains identified as SUNOCONs have suggested extensive and microscopic mixing of elements in the different layers in the explosion (Amari & Zinner 1997; Travaglio et al. 1999). Thus, as an ideal case, the uniform mixing of elements within the He core was considered to investigate dust formation in the ejecta of supernovae (Kozasa et al. 1989a; Todini & Ferrara 2001; Schneider, Ferrara, & Salvaterra 2003a). On the other hand, Douvion et al. (2001b) have suggested that the mixing in the ejecta of the Cas A SNR is knotty rather than microscopic. A simple calculation of molecular diffusion has shown that mixing at the atomic level is impossible before the condensation of dust grains in the ejecta (Deneault, Clayton, & Heger 2003). It is still debated at this moment whether the mixing is macroscopic at the knotty level or microscopic at the atomic level and how large the mixing is that is extended into the ejecta. Therefore, in the following calculation of dust formation we consider two extreme cases for the mixing of elements; one is the unmixed case, with the original onion-like structure, and the other is the mixed case, for which the elements are uniformly mixed within the He core.

2.2. *The Time Evolution of Gas Density and Temperature in the Ejecta*

The time evolution of gas density and temperature strongly affects the number density and size of newly formed grains in the ejecta. As the explosion shock propagates through the star, the reverse shock generated at the interface of layers with different chemical compositions changes the density structure. Although Deneault et al. (2003) show that the reverse shock generated at the He-H interface introduces a very nonhomologous readjustment after $t = 10^6$ s from the explosion, our hydrodynamic calculations including the interaction with the reverse shock have shown that the interaction makes the expansion finally homologous in less than 1 day after the explosion (see Shigeyama & Nomoto 1990). Thus, the time evolution of gas density at a given mass coordinate M_r is calculated by

$$\rho(M_r, t) = \rho(M_r, t_0)\left(\frac{t}{t_0}\right)^{-3}, \quad (1)$$

where the reference time t_0 is 1 day after the explosion. The distribution of gas density within the He core at day 600 after the explosion is shown in Figure 2, where the mass coordinate is normalized to the He core mass and the histogram presentation of the density structure reflects the size of the mesh used in the calculations; Figure 2*a* is for CCSNe (C20 and C25) and HNe (H25) and Figure 2*b* for PISNe (P170 and P200). The gas density within the He cores of CCSNe with the same explosion energy is of almost the same order of magnitude and does not depend so much on the progenitor mass, apart from the detailed structure caused by the propagation of the reverse shock originating at each interface of layers. The gas density in the ejecta of H25 is an order of magnitude lower than that of CCSNe, reflecting the explosion energy of 10 times that of CCSNe. Also, the gas density in the ejecta of P200 is a little bit lower than that in the ejecta of P170, but the gas density within the He core is 10^{-14} to 10^{-13} g cm^{-3} at day 600 after the explosion and is of almost the same order of the magnitude as the gas density in the ejecta of CCSNe, except for the region $M_r \leq 40\ M_\odot$.

The gas temperature in the ejecta is determined by the detailed process of the degradation of γ-rays and X-rays deposited from the radioactive elements. In the previous calculations (Kozasa et al. 1989a, 1991; Todini & Ferrara 2001), the time evolution of gas temperature was approximated by

$$T(M_r, t) = T(M_r, t_0)\left(\frac{t}{t_0}\right)^{3(1-\gamma)}, \quad (2)$$

with a parameter γ, and the reference temperature $T(M_r, t_0)$ was determined by the observations of SN 1987A. However, this method is not applicable for Population III supernovae with no observational data. Therefore, the time evolution of gas temperature is calculated by using the multifrequency radiative transfer code together with the energy equation, taking account of the deposition of energy from radioactive elements (see Iwamoto et al. 2000 for details).

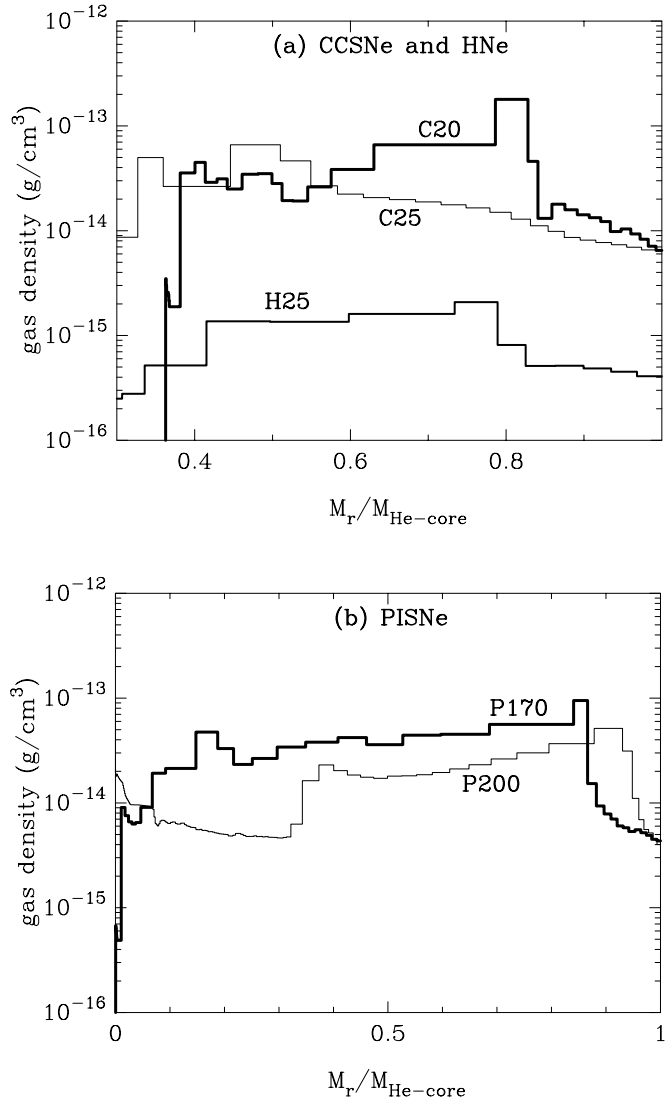

FIG. 2.—Distribution of gas density within the He core at 600 days after the explosion for (*a*) C20, C25, and H25 and (*b*) P170 and P200. Note that the mass coordinate is normalized to the He core mass. [*See the electronic edition of the Journal for a color version of this figure.*]

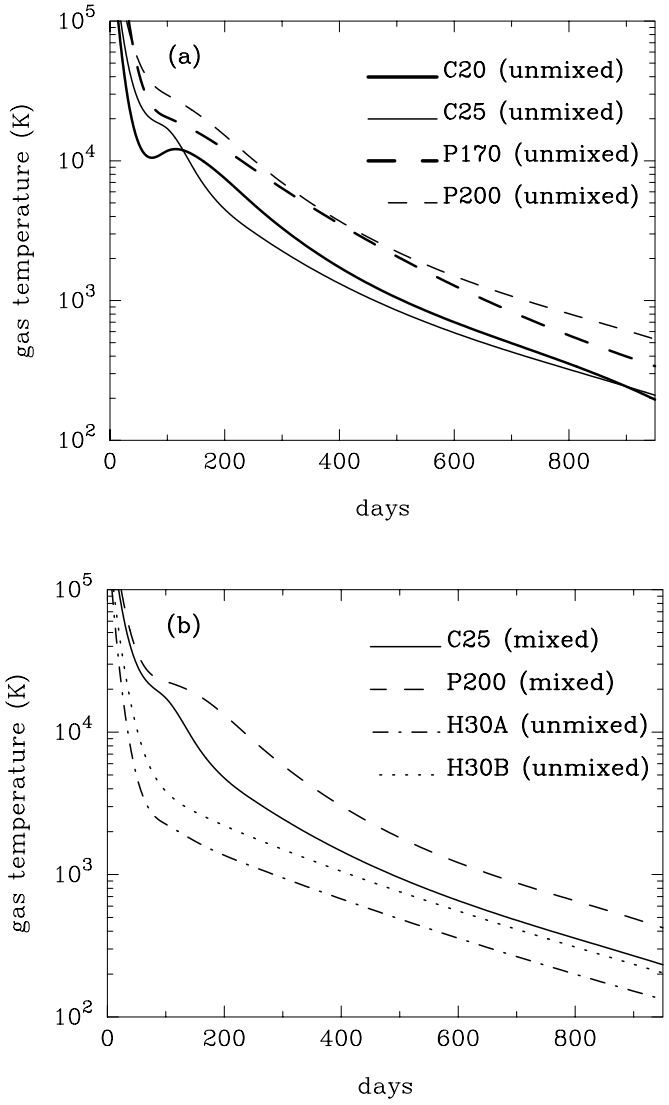

FIG. 3.—Time evolution of gas temperature at a location in the oxygen-rich layer with almost the same elemental composition in the ejecta of CCSNe, PISNe, and HNe. (*a*) At $M_r = 3.7$, 4.6, 56.5, and 64.9 $M_\odot$ for C20, C25, P170, and P200, respectively, in the unmixed ejecta. (*b*) At $M_r = 4.6$ and 64.9 $M_\odot$ for C25 and P200, respectively, in the mixed ejecta and $M_r = 6.8$ $M_\odot$ for H30A and H30B in the unmixed ejecta. [*See the electronic edition of the Journal for a color version of this figure.*]

As an example, Figure 3 shows the time evolution of gas temperature at a location in the oxygen-rich layer with almost the same elemental composition in the ejecta of CCSNe, PISNe, and HNe: Figure 3*a* for the unmixed ejecta of C20 (at $M_r = 3.7$ $M_\odot$), C25 (at $M_r = 4.6$ $M_\odot$), P170 (at $M_r = 56.5$ $M_\odot$), and P200 (at $M_r = 64.9$ $M_\odot$) and Figure 3*b* for the mixed ejecta of C25 (at $M_r = 4.6$ $M_\odot$) and P200 (at $M_r = 64.9$ $M_\odot$) and the unmixed ejecta of H30A (at $M_r = 6.8$ $M_\odot$) and H30B (at $M_r = 6.8$ $M_\odot$). It should be pointed out here that, as can be seen from Figure 3, the temporal evolution of gas temperature in the ejecta is approximately determined only by the explosion energy and the amount of ^{56}Ni in the ejecta and does not heavily depend on the progenitor mass in the mass range considered in this paper. Also, the gas temperature in the mixed ejecta is almost the same as that in the unmixed ejecta, except for the gas temperature around the day 200 after the explosion. The gas temperature in the ejecta of H30, with its large explosion energy, quickly decreases in comparison with that in CCSNe, because X-rays and γ-rays escape easily as a result of the low gas density in the ejecta. The effect of $M(^{56}\mathrm{Ni})$ in the ejecta on the gas temperature is clearly shown by the difference in the gas temperature in the unmixed ejecta between H30A and H30B. The gas temperature in the ejecta of PISNe with a large explosion energies is much higher than that in CCSNe, because the progenitors are massive and a large amount of ^{56}Ni resides in the ejecta.

From Figures 2 and 3, we can easily estimate the condensation time and the behavior of the average radius of a grain species formed in the ejecta of Population III supernovae; if the grains condense around a gas temperature of 1500 K in the oxygen-rich layer, the condensation time t_c after the explosion would be around day 400 for CCSNe, day 600 for PISNe, and day 200 for HNe with the same $M(^{56}\mathrm{Ni})$ as CCSNe. The average radius of the condensate would not be much different, since the average size is roughly proportional to $\rho^{1/3} \propto (1/t_c)$, so long as the abundance of the

elements available for dust formation is the same, which is confirmed by the results of the dust formation calculations given in § 4 and Appendix A. Note that the radiation transfer calculation does not include the radiative cooling of molecules, such as CO and SiO, that act as effective coolants of gas in the ejecta, as demonstrated by Liu & Dalgarno (1995) for SN 1987A. The effect of radiative cooling of molecules would make the condensation time of dust grains earlier and the average radius larger than those presented in § 4. However, the average size and the number density of newly formed grains could not be much different, so long as the condensation time is on the order of 100 days.

3. FORMULATION AND CALCULATION OF DUST FORMATION

3.1. *Formulation of Nucleation and Grain Growth*

In astrophysical environments, dust grains condense via formation of condensation nuclei and their growth through the collisions of gaseous species in a cooling gas outflowing from a star into interstellar space.

The nucleation rate is usually formulated under the condition of the presence of monomer molecule whose chemical composition is the same as the condensate. However, for formation of compound grains of astrophysical interest, such as silicates, no gaseous monomer molecule exists, and it is impossible to derive rigorously the nucleation rate without specifying the chemical pathways and reaction constants. Nevertheless, even if no information on chemical pathways and reaction constants is available for the formation of compound grains, as is discussed by Yamamoto et al. (2001), the nucleation rate can be evaluated by applying the concept of the key species, introduced by Kozasa & Hasegawa (1987), when the net reaction rate is much larger than the decay rate. Under the assumption that the key species, defined as the gaseous species with the least collision frequency among the reactants, controls the kinetics of nucleation and grain growth, the steady state nucleation rate of the jth grain species, $J_j^s(t)$, is given by

$$J_j^s(t) = \alpha_{sj}\Omega_j \left(\frac{2\sigma_j}{\pi m_{1j}}\right)^{1/2} \left(\frac{T}{T_d}\right)^{1/2} \Pi_j c_{1j} \exp\left[-\frac{4}{27}\frac{\mu_j^3}{(\ln S_j)^2}\right] , \tag{3}$$

where α_{sj} is the sticking probability of the key species for the jth grain species, Ω_j is the volume of the condensate per molecule of the key species, and σ_j is the surface energy. We assume $\alpha_{sj} = 1$ in the calculations (see Hasegawa & Kozasa 1988; Kozasa et al. 1996; Chigai, Yamamoto, & Kozasa 1999 for the derivation of steady state nucleation rate). The concentration and the mass of the key species for the jth grain species are denoted by c_{1j} and m_{1j}, respectively. T_d is the temperature of the condensation nuclei, and T is the gas temperature (see Kozasa et al. 1996). The factor Π_j is a function of the partial gas pressures of reactants and products except for the key species (Yamamoto et al. 2001), and we set $\Pi_j = 1$ in the calculations, partly because the appearance of the factor is somehow related to the detailed chemical reaction mechanism at the condensation and partly because the factor can be negligible under the condition that the number of molecules of the key species contained in the condensation nuclei is much larger than unity. The quantity μ_j, representing the energy barrier for nucleation, is defined by $\mu_j = 4\pi a_{0j}^2 \sigma_j / kT_d$, with the hypothetical radius of condensate per molecule of the key species $a_{0j} = \left(3\Omega_j/4\pi\right)^{1/3}$, where k is Boltzmann's constant. We assume that the temperature of the condensation nuclei is the same as the gas temperature in what follows. The supersaturation ratio S_j, taking into account the chemical reaction at the condensation of the jth grain species, is calculated by

$$\ln S_j = -\frac{\Delta G_j^0}{kT} + \sum_i \nu_{ij} \ln P_{ij} , \tag{4}$$

where ΔG_j^0 is the Gibbs free energy of formation of the jth grain species from the reactants per molecule of the key species and P_{ij} are the partial gas pressures of the reactant and product gas species. The stoichiometric coefficients ν_{ij} of the reactants and products are normalized to the key species; ν_{ij} is positive for a reactant and negative for a product (see Kozasa & Hasegawa 1987; Hasegawa & Kozasa 1988).

In the ejecta of supernovae, where the gas cooling time and/or the collision time controlling the process of nucleation and grain growth are comparable to the dynamical timescale, the application of the steady state nucleation rate is questionable. In this paper, following Gail, Keller, & Sedlmayr (1984), we employ the non–steady state nucleation rate $J_j(t)$ evaluated by the equation

$$\frac{\partial}{\partial t}\left[\frac{J_j(t)}{\eta_j}\right] = -\frac{1}{\tau_{*,j}\eta_j}\left[J_j(t) - J_j^s(t)\right] , \tag{5}$$

with the relaxation time toward the steady state $\tau_{*,j}$ defined by

$$\begin{aligned}\tau_{*,j}^{-1} &= 4\pi a_{0j}^2 \alpha_{sj} \left(\frac{kT}{2\pi m_{1j}}\right)^{1/2} c_{1j}(t) \frac{(\ln S_j)^2}{\mu_j} \\ &= \tau_{\mathrm{coll},j}^{-1} \frac{(\ln S_j)^2}{\mu_j}\end{aligned} \tag{6}$$

and $\eta_j = \tau_{\mathrm{coll},j}^{-1}\left(r_{c,j}/a_{0j}\right)^2$, where $\tau_{\mathrm{coll},j}$ is the collision time of the key species and $r_{c,j} = 2a_{0j}\mu_j/3\ln S_j$ is the critical radius for the jth grain species.

Given the nucleation rate $J_j(t)$ at a time t, the process of nucleation and grain growth is described by the two basic equations in a frame comoving with gas. One is the equation of continuity for the key species, given by

$$1 - \frac{c_{1j}(t)}{\tilde{c}_{1j}(t)} = 1 - Y_{1j} = \int_{t_e}^{t} \frac{J_j(t')}{\tilde{c}_{1j}(t')} \frac{4\pi}{3\Omega_j} r_j^3(t, t')\, dt' , \tag{7}$$

where t_e is the equilibrium time, defined as the time at which the supersaturation ratio S_j reaches unity without depletion of the key species, $\tilde{c}_{1j}$ is the nominal concentration of the key species expected without depletion of the key species due to nucleation and grain growth, $Y_{1j} = c_{1j}/\tilde{c}_{1j}$ represents the degree of depletion of the key species due to nucleation and grain growth, and $r_j(t, t')$ is the radius of a grain nucleated at t' and measured at t. Another is the equation of grain growth, given by

$$\frac{dr_j}{dt} = \alpha_{sj}\Omega_j \left(\frac{kT}{2\pi m_{1j}}\right)^{1/2} c_{1j}(t) = \frac{1}{3} a_{0j} \tau_{\mathrm{coll},j}^{-1}(t) . \tag{8}$$

By differentiating equation (7) with t subsequently, the integral equation is reduced to the simultaneous ordinary

equations

$$\frac{dK_j^{(i)}}{dt} = \frac{J_j(t)}{\tilde{c}_{1j}(t)} \frac{4\pi}{3\Omega_j} r_{c,j}^i + iK_j^{(i-1)} \frac{dr_j}{dt} \quad (9)$$

(for $i = 1$–3) and

$$\frac{dK_j^{(0)}}{dt} = \frac{J_j(t)}{\tilde{c}_{1j}(t)} \frac{4\pi}{3\Omega_j} \ . \quad (10)$$

In principle, by solving equations (5), (8), (9), and (10), coupled with the temporal evolution of gas density $\rho(t)$ and temperature $T(t)$ with the number abundances of reactants, the number density $n_{\mathrm{gr},j}(t)$ and volume equivalent average radius $r_{\mathrm{gr},j}(t)$ of the jth grain species are calculated by

$$\frac{n_{\mathrm{gr},j}}{\tilde{c}_{1j}} = a_{0j}^3 K_j^{(0)}(t) \quad (11)$$

and

$$r_{\mathrm{gr},j}^3 = \frac{K_j^{(3)}(t)}{K_j^{(0)}(t)} \ , \quad (12)$$

respectively. Furthermore, the size distribution function $f_j(r)$ of the newly formed jth grain species at a time t is calculated by

$$f_j(r)dr = a_{0j}^3 \tilde{c}_{1j} \frac{dK_j^{(0)}(t')}{dt'} dt' \ , \quad (13)$$

since the grains with radii between r and $r + dr$ are nucleated in the time interval between t' and $t' + dt'$.

3.2. *Calculation of Dust Formation in the Ejecta of Supernovae*

The formation of dust grains in the ejecta of supernovae is calculated by solving equations (5), (8), (9), and (10) with the temporal evolution of gas density and temperature, given the grain species, the chemical reaction at the condensation, and the abundance of the reactants. The formation of CO and SiO molecules prior to the formation of dust grains was observed in the ejecta of SN 1987A (e.g., Bouchet & Danziger 1993). The formation of CO and SiO molecules plays a crucial role in the formation of dust grains, because CO molecules lock the oxygen atoms available for the formation of oxide grains and SiO molecules are considered to be the starting molecules to form silicate grains.

As discussed by Liu & Dalgarno (1994, 1996), in the ejecta of supernovae, these molecules are destroyed by impact with energetic electrons and charge transfer reactions with the ionized inert gaseous atoms, which are created by the decay of radioactive elements whose abundances depend on the elemental composition, as well as on the degree of the mixing in the ejecta. In this paper, to simplify the calculation of dust formation, we assume that the formation of CO and SiO molecules is complete, that is, that no carbon-bearing grain condenses in the region of $C/O < 1$ and no Si-bearing grain, except for oxide grains, condenses in the region of $Si/O < 1$. The effect of incomplete formation of CO molecules has been extensively investigated by Clayton, Liu, & Dalgarno (1999) and Clayton, Deneault, & Meyer (2001), and they have shown that carbon grains can condense even in the region of $C/O < 1$. Also, the formation efficiency of SiO molecules is expected to affect the abundance and the size of Si- and/or Mg-bearing grains. The effect of the formation efficiency of CO and SiO molecules on dust formation in the ejecta is discussed in Appendix B.

The grain species, the chemical reactions at the condensations, and the basic data necessary for dust formation calculations are in Table 2. The Gibbs free energy for formation of a condensate from the reactants is approximated by $\Delta G_j^0/kT = -A/T + B$, and the numerical values of A and B are evaluated by least-squares fitting of the thermodynamic data (Chase et al. 1985). It should be recognized here that what kind of grain species really condenses in a gas with a given elemental composition is determined by the competitive process of formation of each grain species, because formation of a grain species depletes the gaseous atoms and molecules available for the condensation of other grains. So in the calculations, the formation of all possible condensates in Table 2 is taken into account simultaneously.

4. THE RESULTS OF CALCULATIONS AND DISCUSSIONS

In this section, the results of the calculations of dust formation in the ejecta of ordinary CCSNe and PISNe are presented and discussed. The behaviors of nucleation and growth of dust grains are depicted in § 4.1. The detailed results on the condensation times, average radii, and size distribution functions of each grain species formed in the unmixed and mixed ejecta of CCSNe and PISNe are presented and discussed in §§ 4.2 and 4.3, respectively. The dependence of the total mass of newly formed grains and of the mass yield of each grain species on the progenitor mass are given in §§ 4.4 and 4.5, respectively. The effects of the explosion energy, as well as the amount of ^{56}Ni in the unmixed ejecta, on dust formation are investigated in Appendix A, and the effect of the formation efficiency of CO and SiO molecules is discussed in Appendix B.

4.1. *The Behavior of Nucleation and Grain Growth*

Figure 4 depicts the behaviors of nucleation and grain growth as a function of time after the explosion at a location of $M_r = 3.5\ M_\odot$ in the O-Mg-Si layer, with the elemental abundances relative to oxygen $Si/O = 2.97 \times 10^{-2}$, $Mg/O = 8.25 \times 10^{-2}$, and $Al/O = 9.38 \times 10^{-4}$; Figure 4*a* is for the behaviors of nucleation rate $J_j(t)$ and the depletion of the key species Y_{1j}, and Figure 4*b* is for the number density $n_{\mathrm{gr},j}$ and the average radius $r_{\mathrm{gr},j}$. At this location, the expected condensates are Al_2O_3 and Si- and/or Mg-bearing grains. The key species is Al for Al_2O_3 and Mg or SiO for Mg- and/or Si-bearing grains, depending on what kind of grain species really condenses.

As the gas cools down with time, it can be clearly shown from Figure 4 that the nucleation rate rapidly increases with increasing supersaturation ratio and then decreases with the depletion of the key species due to grain growth; thus, the nucleation rate has a maximum at a given time. This is a typical behavior of nucleation and grain growth in a cooling gas. The time at which the nucleation rate reaches the maximum is defined as the

TABLE 2
GRAIN SPECIES CONSIDERED IN THE CALCULATIONS

Grains	Key Species	Chemical Reactions	$A/10^4$ (K)	B	σ_j (ergs cm^{-2})	References for σ_j	a_{0j} (Å)
$Fe_{(s)}$	$Fe_{(g)}$	$Fe_{(g)} \rightarrow Fe_{(s)}$	4.84180	16.5566	1800	1	1.411
$FeS_{(s)}$	$Fe_{(g)}$, $S_{(g)}$	$Fe_{(g)} + S_{(g)} \rightarrow FeS_{(s)}$	9.31326	30.7771	380	2	1.932
$Si_{(s)}$	$Si_{(g)}$	$Si_{(g)} \rightarrow Si_{(s)}$	5.36975	17.4349	800	3	1.684
$Ti_{(s)}$	$Ti_{(g)}$	$Ti_{(g)} \rightarrow Ti_{(s)}$	5.58902	16.6071	1510	3	1.615
$V_{(s)}$	$V_{(g)}$	$V_{(g)} \rightarrow V_{(s)}$	6.15394	17.8702	1697	3	1.490
$Cr_{(s)}$	$Cr_{(g)}$	$Cr_{(g)} \rightarrow Cr_{(s)}$	4.67733	16.7596	1880	3	1.421
$Co_{(s)}$	$Co_{(g)}$	$Co_{(g)} \rightarrow Co_{(s)}$	5.03880	16.8372	1936	3	1.383
$Ni_{(s)}$	$Ni_{(g)}$	$Ni_{(g)} \rightarrow Ni_{(s)}$	5.09130	17.1559	1924	3	1.377
$Cu_{(s)}$	$Cu_{(g)}$	$Cu_{(g)} \rightarrow Cu_{(s)}$	3.97955	14.9083	1300	3	1.412
$C_{(s)}$	$C_{(g)}$	$C_{(g)} \rightarrow C_{(s)}$	8.64726	19.0422	1400	4	1.281
$SiC_{(s)}$	$Si_{(g)}$, $C_{(g)}$	$Si_{(g)} + C_{(g)} \rightarrow SiC_{(s)}$	14.8934	37.3825	1800	5	1.702
$TiC_{(s)}$	$Ti_{(g)}$, $C_{(g)}$	$Ti_{(g)} + C_{(g)} \rightarrow TiC_{(s)}$	16.4696	37.2301	1242	6	1.689
$Al_2O_{3\,(s)}$	$Al_{(g)}$	$2Al_{(g)} + 3O_{(g)} \rightarrow Al_2O_{3\,(s)}$	18.4788	45.3543	690	7	1.718
$MgSiO_{3\,(s)}$	$Mg_{(g)}$, $SiO_{(g)}$	$Mg_{(g)} + SiO_{(g)} + 2O_{(g)} \rightarrow MgSiO_{3\,(s)}$	25.0129	72.0015	400	8	2.319
$Mg_2SiO_{4\,(s)}$	$Mg_{(g)}$	$2Mg_{(g)} + SiO_{(g)} + 3O_{(g)} \rightarrow Mg_2SiO_{4\,(s)}$	18.6200	52.4336	436	8	2.055
	$SiO_{(g)}$	$2Mg_{(g)} + SiO_{(g)} + 3O_{(g)} \rightarrow Mg_2SiO_{4\,(s)}$	37.2400	104.872	436	8	2.589
$SiO_{2\,(s)}$	$SiO_{(g)}$	$SiO_{(g)} + O_{(g)} \rightarrow SiO_{2\,(s)}$	12.6028	38.1507	605	7	2.080
$MgO_{(s)}$	$Mg_{(g)}$	$Mg_{(g)} + O_{(g)} \rightarrow MgO_{(s)}$	11.9237	33.1593	1100	7	1.646
$Fe_3O_{4\,(s)}$	$Fe_{(g)}$	$3Fe_{(g)} + 4O_{(g)} \rightarrow Fe_3O_{4\,(s)}$	13.2889	39.1687	400	7	1.805
$FeO_{(s)}$	$Fe_{(g)}$	$Fe_{(g)} + O_{(g)} \rightarrow FeO_{(s)}$	11.1290	31.9850	580	7	1.682

NOTES.—The key species is defined as the gaseous species with the least collisional frequency among the reactants. The subscripts "(s)" and "(g)" denote condensate and gas species, respectively. The Gibbs free energy ΔG_j^0 for formation of the condensate from the reactants per molecule of the key species is approximated by $\Delta G_j^0/kT = -A/T + B$, and the numerical values A and B are evaluated by least-squares fitting of the thermodynamic data (Chase et al. 1985) in the range of temperatures of interest; σ_j is the surface energy of the condensate, and a_{0j} is the hypothetical radius of the condensate per molecule of the key species, whose values are calculated from the molar volumes tabulated by Robie & Waldbaum 1968.

REFERENCES.—(1) Elliott, Gleiser, & Ramakrishna 1963; (2) Kozasa & Hasegawa 1988; (3) Elliott & Gleiser 1960; (4) Tabak et al. 1975; (5) Kozasa et al. 1996; (6) Rhee 1970; (7) Overbury, Bertrand, & Somorjai 1975; (8) Boni & Derge 1956.

condensation time. At this location, Al_2O_3 grains condense first at day 400, then Mg_2SiO_4 grains condense, consuming the key species SiO, at day 421, and finally the remaining Mg atoms are locked into MgO grains at day 439. Also, it should be noted that each grain grows to the final radius in a very short time interval: less than 20 days after the condensation time.

Furthermore, we can see from Figure 4 that a smaller abundance of the key species leads to a larger number density of condensation nuclei, with a broad peak of the nucleation rate, and results in a small average radius. Thus, the abundance of the key species is very sensitive to the number density and average radius of newly formed grains, which is well reflected by the size distribution function of grains given in Figure 5, in Figure 5*a* at $M_r = 3.5\ M_\odot$ and in Figure 5*b* at $M_r = 4.0\ M_\odot$, where the abundances of Si, Mg, and Al are more than an order of magnitude smaller than at $M_r = 3.5\ M_\odot$: $\mathrm{Si/O} = 1.50 \times 10^{-4}$, $\mathrm{Mg/O} = 6.40 \times 10^{-3}$, and $\mathrm{Al/O} = 3.95 \times 10^{-5}$. At $M_r = 4.0\ M_\odot$, the smaller abundance of the key species SiO for the formation of Mg_2SiO_4 grains results in a larger number of condensation nuclei with a very broad peak of the nucleation rate, corresponding to a widespread size distribution, which is true for the formation of Al_2O_3 grains. On the other hand, the size distribution function of MgO grains at $M_r = 4.0\ M_\odot$ is almost the same as that at $M_r = 3.5\ M_\odot$, because the abundance of Mg, being the key species for the formation of MgO and remaining after the formation of Mg_2SiO_4, is only a factor of 4 smaller at $M_r = 4\ M_\odot$ than at $M_r = 3.5\ M_\odot$. Note that the size distribution function of a grain species formed at a location is approximately lognormal so long as the average size is larger than $\sim 0.01\ \mu$m.

4.2. *Dust Formation in the Unmixed Ejecta of CCSNe and PISNe*

In the unmixed ejecta of supernovae, a variety of grain species condense in each layer, corresponding to the difference in the elemental composition. Figures 6*a* and 6*b* show the condensation times of dust grains formed in the unmixed ejecta of C20 and P170, respectively. At first, carbon grains condense in the He layer, which is followed by the condensation of Al_2O_3 and Mg silicates (Mg_2SiO_4 and $MgSiO_3$) in the oxygen-rich layer, MgO in the O-Mg-Si layer, SiO_2 in the O-Si-Mg layer, Si and FeS in the Si-S-Fe layer, and Fe in the innermost Fe-Si-S layer in this sequence. Note that in the O-Si-Mg layer, SiO_2 grains condense from SiO molecules left over after the formation of Mg silicate grains; MgO grains condense from Mg atoms remaining in the O-Mg-Si layer. The major grain species are Mg_2SiO_4 and MgO in the O-Mg-Si layer and $MgSiO_3$ and SiO_2 in the O-Si-Mg layer. In the ejecta of C20, Si grains condense in the innermost region of the He layer because a significant amount of Si atoms are present around the interface between the He layer and the oxygen-rich layer (see Fig. 1*a*), but no SiC grains condense in this region. Anyway, in the unmixed ejecta of C20 and P170, the grain species condensed in the ejecta are the same. Also, metallic Cr and Ni grains do not condense significantly in the Fe-Si-S layer of both ejecta because of low number density, as well as the high energy barrier for nucleation.

The condensation time generally depends not only on the temporal evolution of gas temperature, but also on the concentration of the key species at the formation site. On the other hand, given the time evolution of gas temperature,

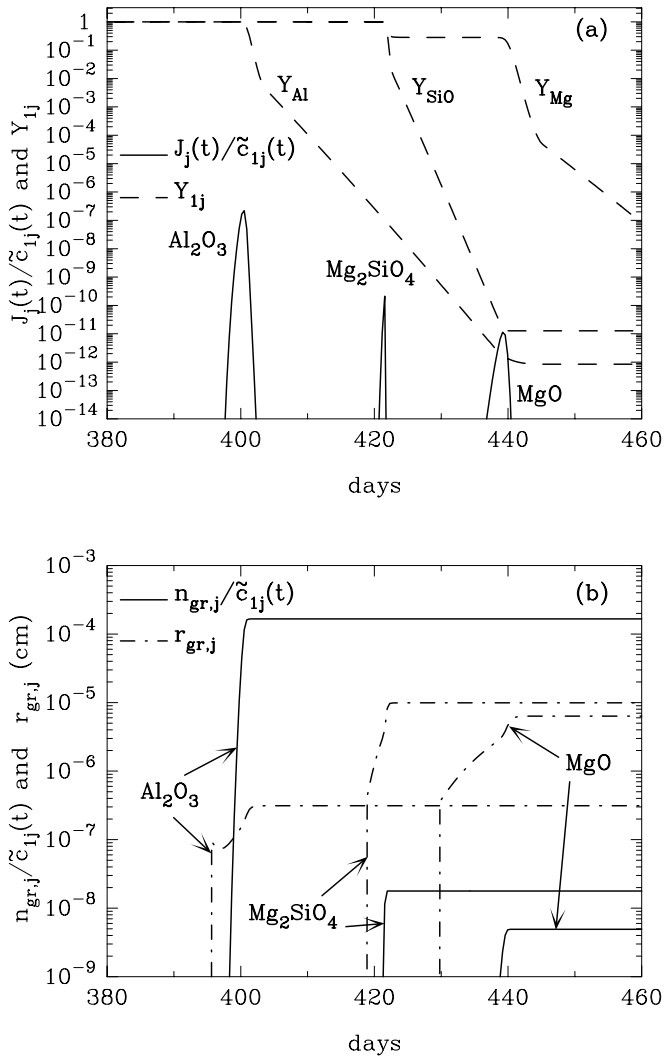

FIG. 4.—Behaviors of nucleation and growth of each grain species condensed at $M_r = 3.5\ M_\odot$ in the O-Mg-Si layer of the unmixed ejecta for C20. (*a*) Time evolution of the nucleation rate $J_j(t)$ normalized to $\tilde{c}_{1j}(t)$ (*solid line*) and the depletion of key species Y_{1j} (*dashed line*). (*b*) Time evolution of the number density $n_{gr,j}$ normalized to $\tilde{c}_{1j}(t)$ (*solid line*) and the average grain radius $r_{gr,j}$ (*dot-dashed line*). The number abundances of dust-forming elements relative to oxygen at this location are $Si/O = 2.97 \times 10^{-2}$, $Mg/O = 8.25 \times 10^{-2}$, and $Al/O = 9.38 \times 10^{-4}$. [*See the electronic edition of the Journal for a color version of this figure.*]

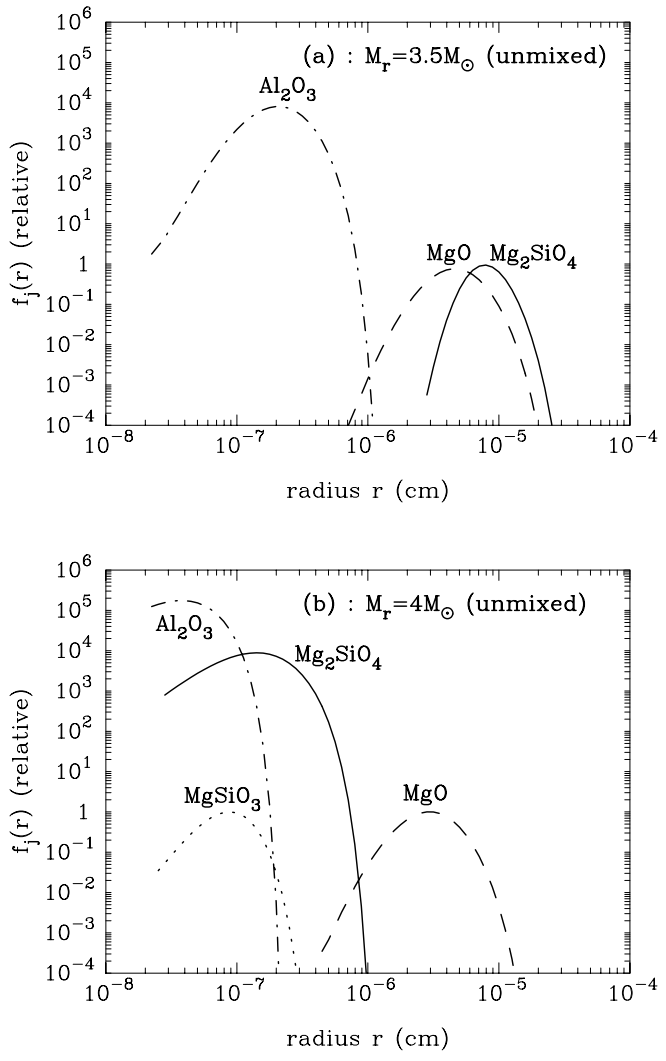

FIG. 5.—Size distribution function of each grain species formed at a location in the O-Mg-Si layer of the unmixed ejecta for C20 at (*a*) $M_r = 3.5\ M_\odot$ and (*b*) $M_r = 4\ M_\odot$, with $Si/O = 1.50 \times 10^{-4}$, $Mg/O = 6.40 \times 10^{-3}$, and $Al/O = 3.95 \times 10^{-5}$. [*See the electronic edition of the Journal for a color version of this figure.*]

the condensation temperature, defined as the gas temperature at the condensation time, depends only on the concentration of the key species; the condensation temperature decreases with decreasing the concentration. In the unmixed ejecta of CCSNe and PISNe, the condensation temperature does not heavily depend on the progenitor mass: ~1900 K for carbon, 1600–1700 K for Al_2O_3, 1400–1500 K for Mg silicates, 1350–1450 K for MgO, 1300–1400 K for SiO_2, 1100–1200 K for Si, 1000–1100 K for FeS, and 800–850 K for Fe. The reason is as follows: as described in § 2, the concentration of the key species is a few times larger in the ejecta of PISNe than in that of CCSNe, and the elemental composition in each layer and the gas density at a given time are not significantly different between CCSNe and PISNe. On the other hand, the gas temperature in the ejecta of PISNe is higher than that of CCSNe. Thus, as can be seen from Figure 6, the condensation time of each grain species in the ejecta of PISNe is delayed about 150 days, in comparison with that of CCSNe. Anyway, dust grains condense in the ejecta of ordinary CCSNe around day 300–600 after the explosion and around day 500–800 in the ejecta of PISNe, which is almost independent of the progenitor mass.

Figures 7*a* and 7*b* show the average radius of each grain species in the ejecta of C20 and P170, respectively. The average radius of each grain species well reflects the concentration of the key species at the condensation time and heavily depends on the elemental composition and the gas density at the formation site in the ejecta. In the ejecta of C20, the average radii of Fe and Si condensed in the innermost region are relatively large: about 0.2 μm for Fe and 0.4 μm for Si. The range of the average radius spans about an order of magnitude for carbon, Al_2O_3, SiO_2, and FeS, whose maximum radii are 0.4, 0.004, 0.1, and 0.06 μm, respectively. The range spans more than 2 orders of magnitude for MgO, Mg_2SiO_4, and $MgSiO_3$, with maximum radii of 0.2, 0.1, and 0.5 μm, respectively. In the ejecta of P170, the average radius of each grain species is a little smaller than that in the

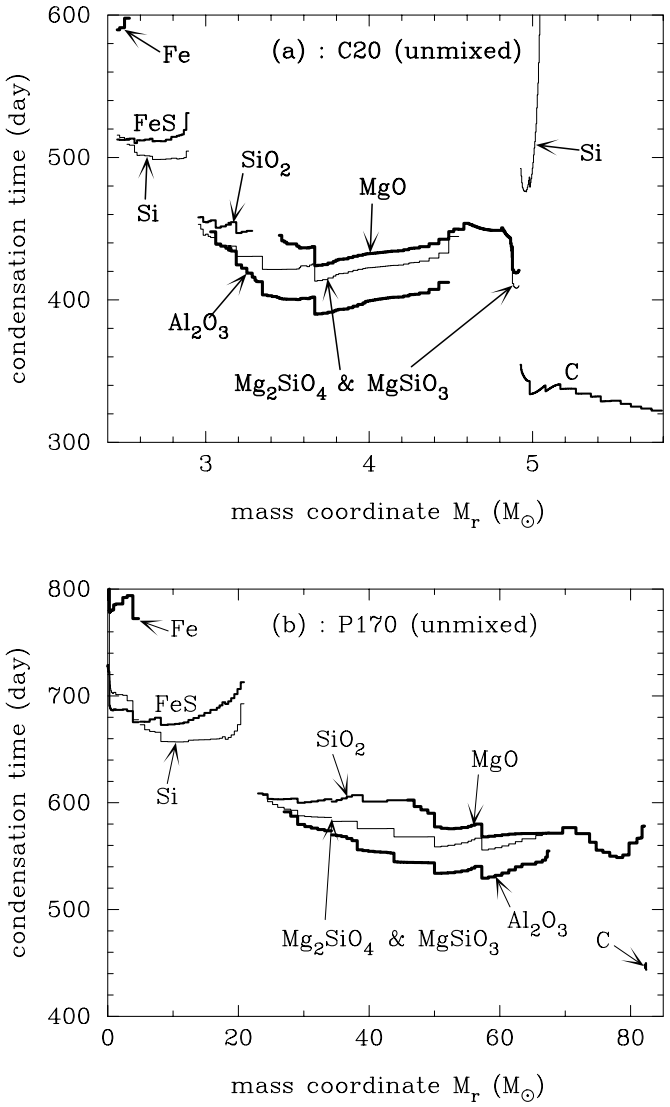

FIG. 6.—Condensation times of dust grains formed in the unmixed ejecta for (*a*) C20 and (*b*) P170. [*See the electronic edition of the Journal for a color version of this figure.*]

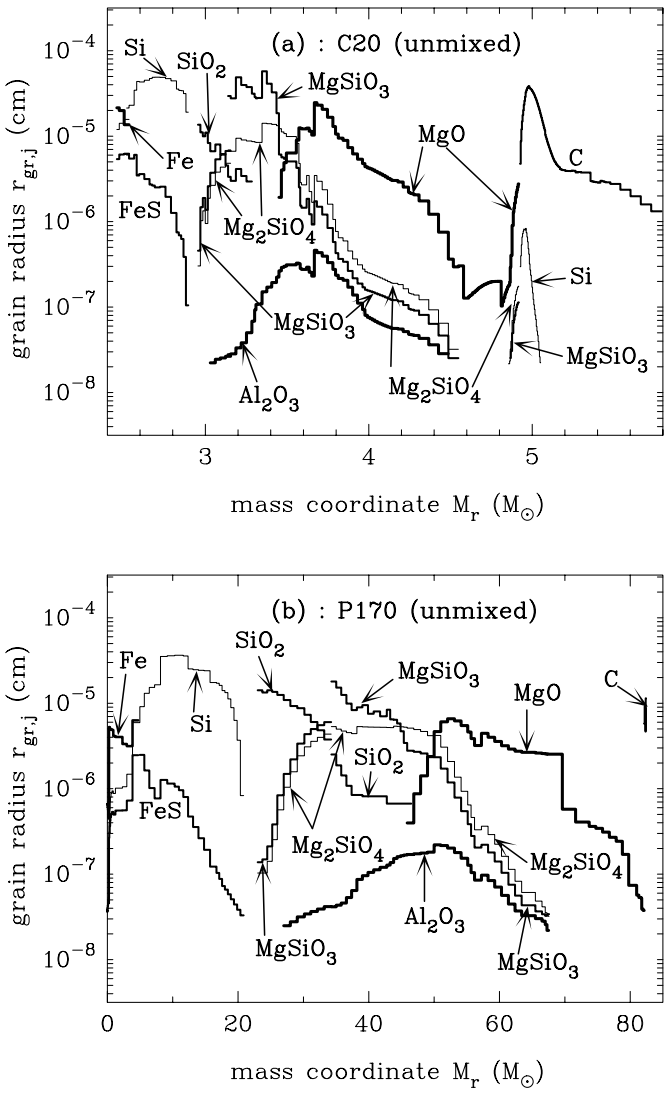

FIG. 7.—Average radii of dust grains formed in the unmixed ejecta for (*a*) C20 and (*b*) P170. [*See the electronic edition of the Journal for a color version of this figure.*]

ejecta of C20, but the difference is not significant, except for Fe, FeS, and Si condensed in the Fe-Si-S layer, where the gas density is substantially lower than that in the ejecta of C20 (see Fig. 2). The average radii of dust grains formed in the unmixed ejecta are limited to less than 1 μm.

The size distribution functions of newly formed grains in the ejecta of C20 and P170 are given in Figures 8*a* and 8*b*, respectively. As is shown in § 4.1, the size distribution function at a location is approximately lognormal for a grain species with an average radius larger than $\sim$0.01 μm. However, the size distribution function of a grain species summed up over the formation region does not keep the original shape at the formation site, reflecting the difference in the elemental composition and gas density in the formation region. Generally, for a grain species whose formation region is widespread in the ejecta and whose average radius spans more than an order of magnitude, the size distribution function completely deviates from the original lognormal shape, which is true for MgO, Mg_2SiO_4, $MgSiO_3$, and FeS grains. Although the average size of carbon grains ranges from 0.01 to 0.4 μm in the ejecta of C20, the size distribution function appears lognormal because the large grains formed in the innermost region of the He layer do not contribute to the size distribution function, as a result of their small numbers relative to the small grains condensed in the outer He layer. The size distribution functions of SiO_2 and Fe in the ejecta of C20 are approximately lognormal. Si grains show a bimodal distribution function with large grains condensed inside the Si-S-Fe layer and smaller ones condensed around the interface between the He and O-Mg-Si layers. In the ejecta of P170, the behavior of the summed-up size distribution function of each grain species is the same as that in the ejecta of C20. However, in the ejecta of P170, the bimodality of Si stems from the wide span of average radii arising from the density variation within the Fe-Si-S layer.

The size distribution function summed up over all grain species formed within the He core is shown by the thick curve in Figure 8. The straight lines represent power-law formulae with indexes of $\alpha = -3.5$ and -2.5. As can be seen from Figure 8, in both cases the size distribution summed up over all grain species is well fitted with a power-law

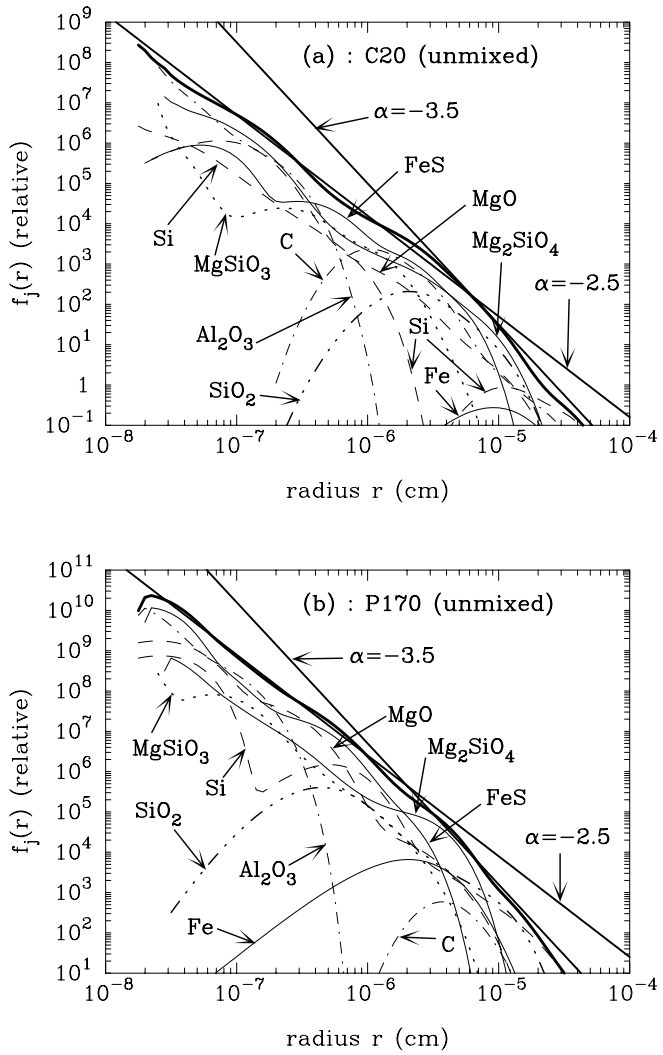

FIG. 8.—Size distribution function of each grain species summed up over the formation region in the unmixed ejecta for (*a*) C20 and (*b*) P170. The thick curve represents the size distribution function summed up over all grain species, and the straight lines indicate power-law formulae with indexes of $\alpha = -2.5$ and -3.5. [*See the electronic edition of the Journal for a color version of this figure.*]

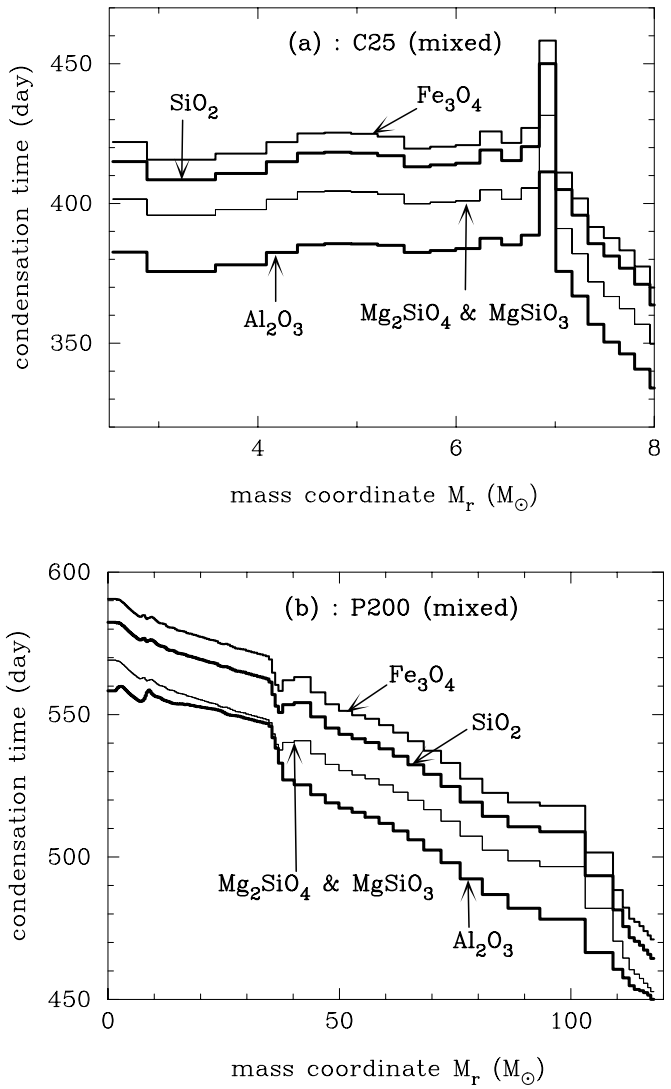

FIG. 9.—Condensation times of dust grains formed in the mixed ejecta for (*a*) C25 and (*b*) P200. [*See the electronic edition of the Journal for a color version of this figure.*]

formula whose index is -3.5 for the larger size and -2.5 for smaller one, which is different from the conventional MRN size distribution function (Mathis, Rumpl, & Nordsieck 1977) used in the astrophysical literature. The radius at the crossover point is 0.06 μm for C20 and 0.02 μm for P170. Although in this subsection only one model each for CCSNe and PISNe is presented, the behaviors of dust formation and the average size, as well as the size distribution function described above, are almost the same for the other models, being independent of the progenitor mass.

4.3. *Dust Formation in the Uniformly Mixed Ejecta of CCSNe and PISNe*

This subsection presents the results of the dust formation calculations in the ejecta with the elemental composition uniformly mixed within the He core, as an extreme case. In the calculations we assume that the density structure in the ejecta is not affected by mixing, since the numerical simulation suggested that the Rayleigh-Taylor instability produces the clumpy structure, but the gas density does not change much on average (Hachisu et al. 1990).

Under the assumption that the formation of CO molecules is complete, only oxide grains condense in the uniformly mixed ejecta, because the ejecta is oxygen-rich. Figure 9 shows the condensation time of each grain species formed in the ejecta, Figure 9*a* for C25 and Figure 9*b* for P200. In both models, Al_2O_3, Mg silicates (Mg_2SiO_4 and $MgSiO_3$), SiO_2, and Fe_3O_4 grains condense in that order. Unlike in the unmixed ejecta, no MgO grain condenses, because Si > Mg in the uniformly mixed ejecta, and all iron atoms are locked into Fe_3O_4 grains. Except for the inner- and outermost regions of P200, the condensation temperature of each dust grain is almost the same within the He core: 1550–1600 K for Al_2O_3, 1450 K for Mg silicates, 1350 K for SiO_2, and 1300–1350 K for Fe_3O_4.

In the ejecta of C25, the gas temperature decreases more rapidly in the outer region than in the inner region of $M_r \leq 6.8\ M_\odot$, where the gas temperature at a time t is almost the same. Thus, well reflecting the temperature structure, in the ejecta of C25, Al_2O_3 grains start to condense in

the outer edge of the He core at day 330 after the explosion, Mg silicate grains at day 350, SiO_2 grains at day 364, and Fe_3O_4 at day 370. In the region of $M_r \leq 6.8\ M_\odot$, each grain species condenses at almost the same time: Al_2O_3 around day 385, Mg silicates around day 400, SiO_2 around day 415, and Fe_3O_4 around day 420. Unlike the formation of dust grains in the unmixed ejecta, all dust grains condense within 100 days after the onset of dust formation. On the other hand, in the ejecta of P200, the condensation time of each grain species increases with a decrease in the mass coordinate, because the gas density gradually decreases with decreasing M_r: Al_2O_3 grains from day 450 to day 560, Mg silicate grains from day 450 to day 570, SiO_2 grains from day 465 to day 583, and Fe_3O_4 grains from day 470 to day 590. In the ejecta of P200, the condensation times of dust grains are about 150 days later than those in the ejecta of C25, since the gas temperature at a given time is higher than that of C25.

As shown in Figures 10*a* for C25 and 10*b* for P200, the range of average radius of each grain species spans less than an order of magnitude throughout the He core. Given the same elemental composition within the He core, the average radius depends not only on the density structure of the gas, but also on the time evolution of the gas temperature; in the outer region of the He core, the gas density is lower than in the inner region, but the gas temperature decreases faster in the outer region, which compensates for the decrease in gas density at the condensation time. In the inner region of P200, the gas temperature is almost the same, being independent of M_r, and the variation of the gas density is less than an order of magnitude. In the mixed ejecta of C25, the average radii of SiO_2 and Mg silicates are a few hundredths of a micron, with a maximum of 0.1 μm for SiO_2, 0.05 μm for Mg_2SiO_4, and 0.07 μm for $MgSiO_3$. The average radii of Fe_3O_4 and Al_2O_3 are small: several tens of angstroms for Fe_3O_4 and several angstroms for Al_2O_3, consistent with the results of Todini & Ferrara (2001). Despite the fact that the gas temperature in the mixed ejecta of P200 is higher than that in C25, the average radius of each grain species formed in the region of $M_r > 40\ M_\odot$ is almost the same as that in the ejecta of C25, because the abundance of the key species of dust grains is a few times larger in P200 than in C25. The low density in the region of $M_r < 40\ M_\odot$ of P200 (see Fig. 2*b*) results in a smaller average radius for each grain species.

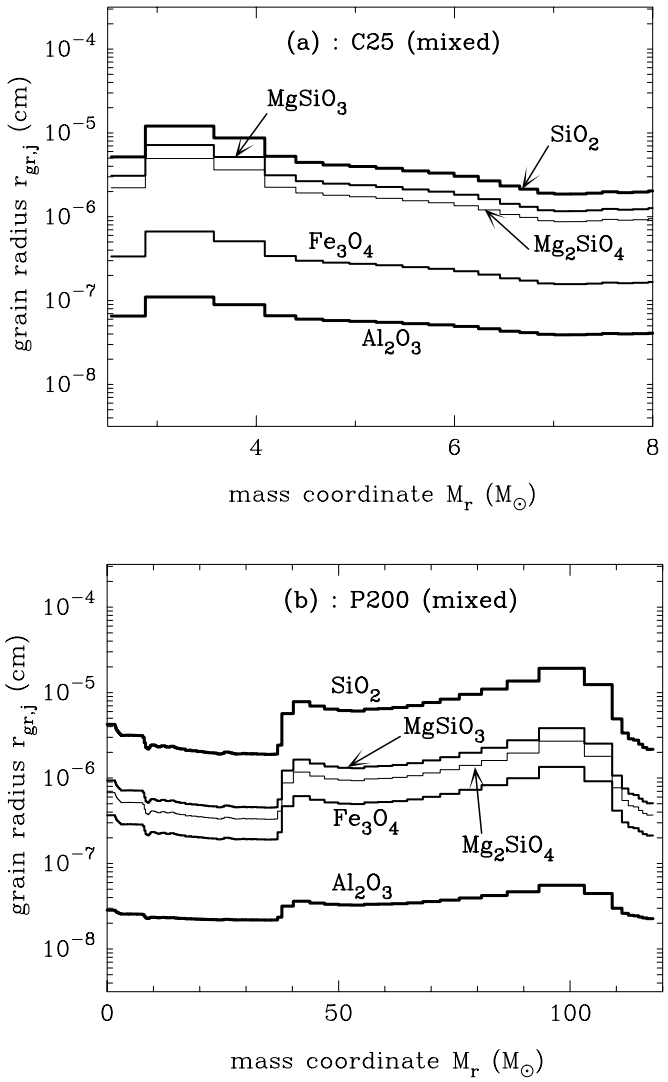

FIG. 10.—Average radii of dust grains formed in the mixed ejecta for (*a*) C25 and (*b*) P200. [*See the electronic edition of the Journal for a color version of this figure.*]

Figure 11 shows the size distribution function of each dust grain formed in the mixed ejecta, Figure 11*a* for C25 and Figure 11*b* for P200. Except for Al_2O_3 grains with a very small average radius, in both models the size distribution functions of Mg_2SiO_4, $MgSiO_3$, SiO_2, and Fe_3O_4 grains tend to be approximately lognormal because of the narrow size range of each grain species. The size distribution function summed up over all grain species is also fitted with a power-law formula, whose index is -3.5 for radii larger than 0.004 μm in P200 and -2.5 for radii smaller than 0.02 μm in C25. The deviation from the power-law formula is distinctive for the larger size in model C25, because only SiO_2 grains with a lognormal distribution function contribute to the larger size. However, this is an untypical case for the behavior of the summed-up size distribution function. Here it should be addressed that, irrespective of the progenitor mass, the size distribution function summed up over all grain species newly formed in the ejecta with and without mixing is approximated by power-law distribution whose index is -3.5 for larger radii and -2.5 for smaller one, although the radius at the crossover point depends on the model of supernovae, with a range from 0.004 to 0.1 μm.

4.4. *The Amount of Freshly Formed Dust Grains*

Figure 12 shows the total mass of dust grains produced in the ejecta versus the progenitor mass, Figure 12*a* for CCSNe and Figure 12*b* for PISNe, where triangles denote the results of calculations for the unmixed ejecta and squares those for the mixed ejecta. In Figure 12*a*, as a reference, the results of calculations in the unmixed ejecta of HNe are also plotted as crosses for H25A and H30A and as circles for H25B and H30B. The straight lines in Figures 12*a* and 12*b* are for the linear least-squares fits to the calculated mass for ordinary CCSNe and linearly connect the two data points for PISNe, respectively: the solid line for the unmixed ejecta and the dashed line for the mixed ejecta.

The total mass of newly formed grains increases with increasing progenitor mass in both the unmixed and mixed ejecta of CCSNe and PISNe. In the unmixed ejecta of ordinary CCSNe, the total dust mass is 0.57 $M_\odot$ for C20 and

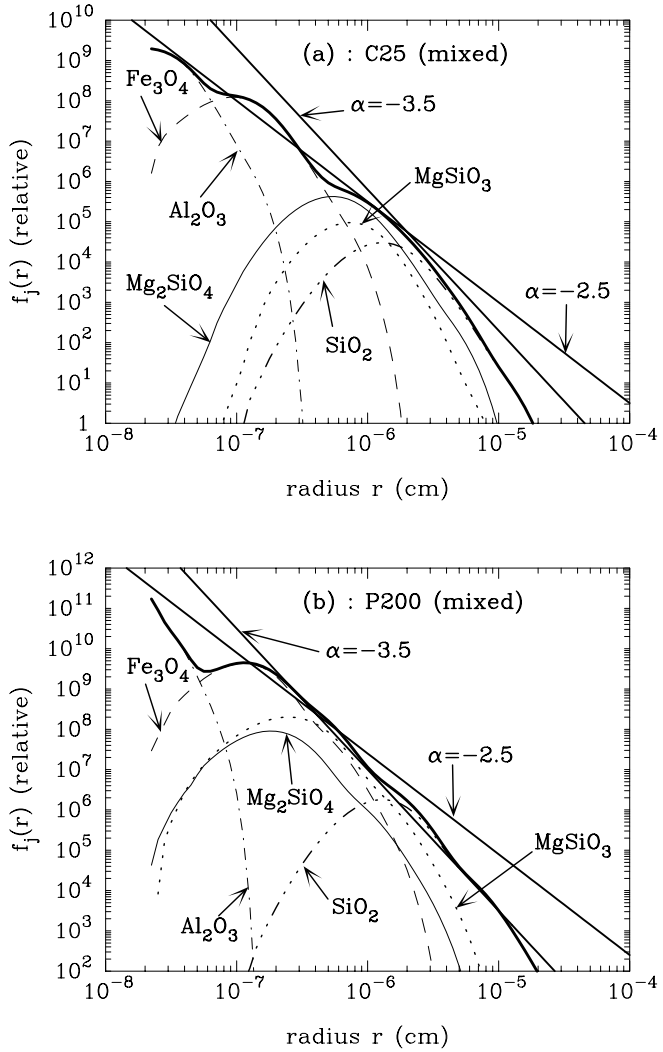

FIG. 11.—Same as Fig. 8, but in the uniformly mixed ejecta for (*a*) C25 and (*b*) P200. [*See the electronic edition of the Journal for a color version of this figure.*]

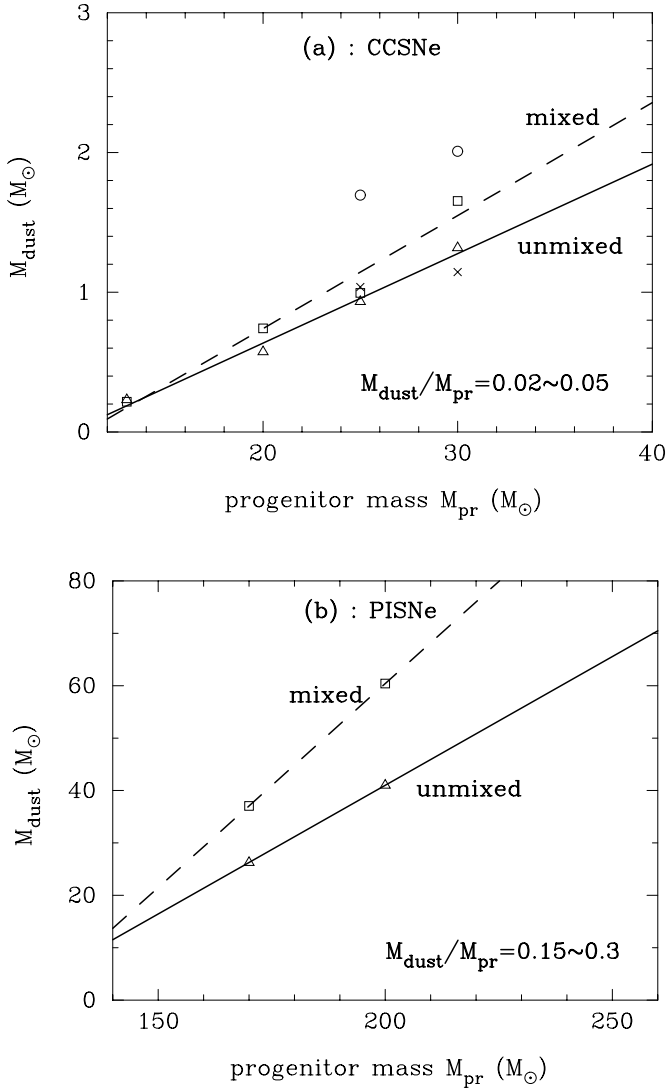

FIG. 12.—Total mass of dust grains formed in the unmixed (*triangles*) and mixed (*squares*) ejecta of CCSNe and PISNe vs. progenitor mass M_{pr} for (*a*) CCSNe and (*b*) PISNe. Lines indicate the least-squares fits to the calculated mass in the unmixed (*solid line*) and mixed (*dashed line*) ejecta of CCSNe in (*a*) and connect the calculated masses for PISNe in (*b*). Also, in (*a*) the total mass of dust grains produced in the unmixed ejecta of HNe is plotted as crosses (H25A and H30A) and circles (H25B and H30B). [*See the electronic edition of the Journal for a color version of this figure.*]

1.32 $M_\odot$ for C30. It is generally expected that the dust mass is larger in the mixed ejecta than in the unmixed ejecta, because many more oxygen atoms are locked into dust grains in the mixed ejecta. However, in the mixed ejecta of C13, the total mass of dust grains is 0.22 $M_\odot$, a little smaller than the dust mass 0.23 $M_\odot$ in the unmixed ejecta. The reason is that in the mixed ejecta of C13, the formation of CO molecules consuming the oxygen atoms available for oxide grains limits the amount of oxide grains; in this case, a small amount of Si and FeS grains condense instead of SiO_2 and Fe_3O_4 grains. Also in model C25, the dust mass in the mixed ejecta is not much different from that in the unmixed ejecta, because in that model the comparatively massive He layer somehow depresses the increase in the amount of mass available for the formation of oxide grains within the oxygen-rich layer.

In the unmixed ejecta of HNe with the same $M(^{56}\mathrm{Ni}) = 0.07\ M_\odot$ as CCSNe, H25A and H30A produce almost the same dust mass as C25 and C30, respectively. On the other hand, with a deep mass cut corresponding to $M(^{56}\mathrm{Ni}) = 0.7\ M_\odot$, H25B and H30B produce about 0.7 $M_\odot$ more dust than C25 and C30, respectively. In the ejecta of the ordinary CCSNe, the ratio of dust mass to progenitor mass is 0.02–0.05, which increases with increasing progenitor mass. Although the total mass of newly formed grains depends on the detailed elemental composition in the ejecta, as well as the position of mass cut, in general the total mass produced in the mixed ejecta becomes larger than that in the unmixed ejecta with increasing M_{pr}.

PISNe, for which the progenitors are very massive and are completely disrupted, produce much more dust than CCSNe. For model P200, the total mass of newly formed grains is ~40 $M_\odot$ in the unmixed ejecta and ~60 $M_\odot$ in the mixed ejecta. The mass ratio of newly formed grains to the progenitor mass for PISNe reaches 0.15–0.3 at least, and the ratio increases with increasing progenitor mass. Therefore, in the early universe, much more dust could be produced and injected into interstellar space if very massive stars populated the first generation of stars.

4.5. *The Mass Yield of Each Grain Species*

Figures 13 and 14 present the mass yield of each grain species versus the progenitor mass $M_{\rm pr}$ in the unmixed ejecta and mixed ejecta, respectively, Figures 13*a* and 14*a* for CCSNe and Figures 13*b* and 14*b* for PISNe. The smooth curves in Figures 13*a* and 14*a* are for the least-squares spline fits to the calculated values for CCSNe, and those in Figures 13*b* and 14*b* represent, in loglinear scale, the straight lines connecting the two calculated values in linear scale for PISNe. Thus, for PISNe the mass yield for a given progenitor mass should be taken as a nominal value.

In the unmixed ejecta of CCSNe (Fig. 13*a*), with increasing $M_{\rm pr}$ the mass yield of carbon grains, apart from a small fluctuation, somehow increases up to around $M_{\rm pr} = 25\ M_\odot$ and then decreases, while the yields of other grain species, except for Fe, increase. The grain species contributing to the total dust mass heavily depend on the progenitor mass for

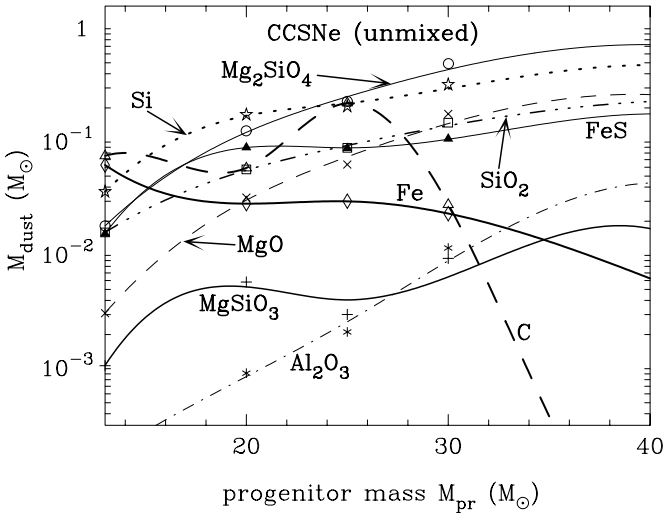

FIG. 13*a*

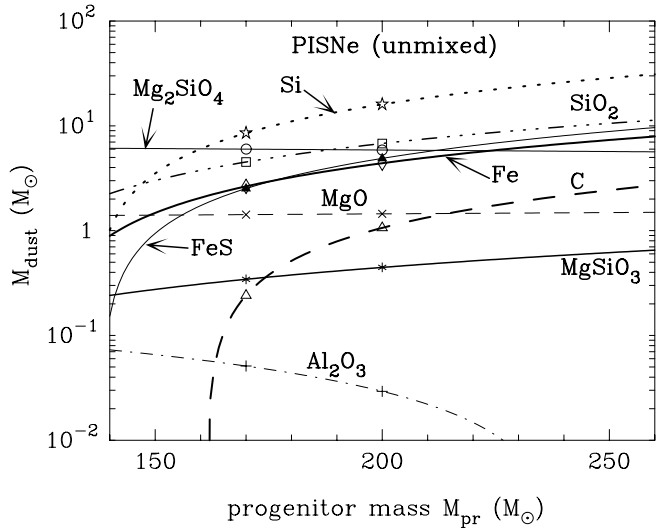

FIG. 13*b*

FIG. 13.—Mass yield of each dust grain formed in the unmixed ejecta for (*a*) CCSNe and (*b*) PISNe. In (*a*) the curves indicate the least-squares spline fits to the calculated yields, and in (*b*) they represent the straight lines connecting the calculated yields in linear scale. [*See the electronic edition of the Journal for a color version of this figure.*]

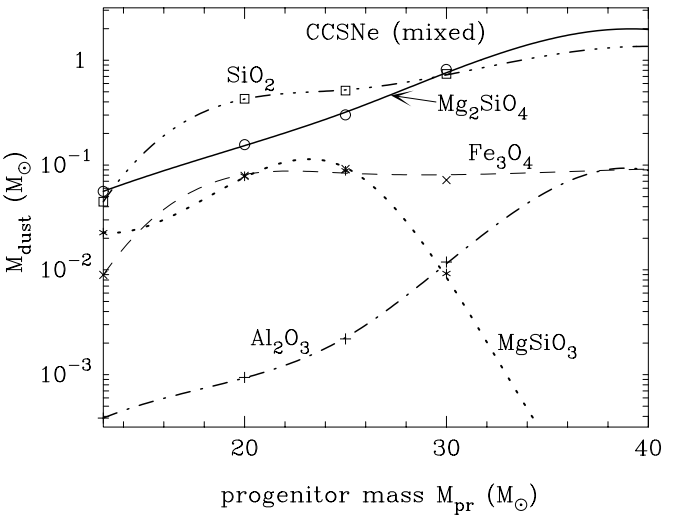

FIG. 14*a*

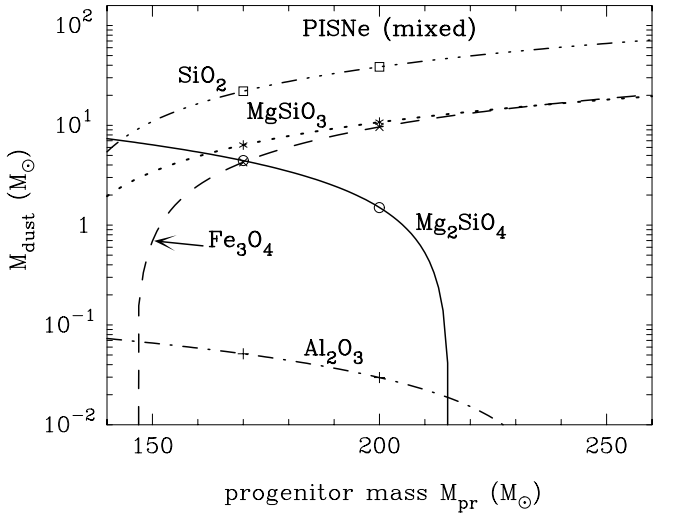

FIG. 14*b*

FIG. 14.—Same as Fig. 13, but in the mixed ejecta for (*a*) CCSNe and (*b*) PISNe. [*See the electronic edition of the Journal for a color version of this figure.*]

$M_{\rm pr} \leq 28\ M_\odot$; in the ejecta with $M_{\rm pr} < 15\ M_\odot$, the major grain species in mass are carbon, Fe, and Si, with an average radius $\geq 0.1\ \mu$m. With increasing $M_{\rm pr}$, the masses of the oxygen-rich layer and the Si-S-Fe layer increase. Therefore, the yields of Si and Mg_2SiO_4 increase, and the mass of FeS also increases, together with a decrease in the mass of Fe. Around $M_{\rm pr} = 20\ M_\odot$, Mg_2SiO_4, Si, and FeS grains tend to dominate the mass abundance. Around $M_{\rm pr} = 25\ M_\odot$, the major grain species are Mg_2SiO_4, Si, and C. The mass abundances of FeS, SiO_2, and MgO grains are larger than that of carbon grains for $M_{\rm pr} \geq 28\ M_\odot$, and Mg_2SiO_4 and Si are the major grain species, followed by MgO, SiO_2, and FeS. Although the masses of Al_2O_3 and $MgSiO_3$ grains increase with $M_{\rm pr}$, their mass fractions are limited to less than 10^{-2}.

The masses of Mg_2SiO_4 and MgO grains per supernova are almost constant in the unmixed ejecta of PISNe, being almost independent of the progenitor mass (see Fig. 13*b*): $M(Mg_2SiO_4) \simeq 6\ M_\odot$ and slightly decreases with increasing $M_{\rm pr}$, and $M({\rm MgO}) = 1.4\ M_\odot$. When the progenitor mass is smaller than 160 $M_\odot$, Mg_2SiO_4, Si, and SiO_2 are the major

grain species contributing to the total mass. In contrast to the case in unmixed ejecta of CCSNe, the mass fraction of carbon grains is less than 5×10^{-2}, although the mass of carbon grains increases with increasing $M_{\rm pr}$. It should be noted here that for $M_{\rm pr} > 160\ M_\odot$, the most abundant grain species in the unmixed ejecta of PISNe is Si, followed by SiO_2, because the masses of the Si-S-Fe and O-Si-Mg layers increase with increasing $M_{\rm pr}$. Also, the mass fractions of the iron-bearing grains (Fe and FeS) produced within the Si-S-Fe and Fe-Si-S layers are larger than those of the Mg_2SiO_4 grains for $M_{\rm pr} > 220\ M_\odot$.

In the mixed ejecta of CCSNe (see Fig. 14*a*), SiO_2 and Mg_2SiO_4 grains mainly contribute to the total dust mass for $M_{\rm pr} \leq 15\ M_\odot$. The mass of Fe_3O_4 for $M_{\rm pr} \geq 20\ M_\odot$ is $\sim$0.09 $M_\odot$, being almost independent of the progenitor mass. With increasing $M_{\rm pr}$, the mass of Mg_2SiO_4 increases and becomes the same as that of SiO_2 at $M_{\rm pr} = 30\ M_\odot$. The dust mass of massive CCSNe with $M_{\rm pr} \geq 25\ M_\odot$ is dominated by SiO_2 and Mg_2SiO_4 grains. Although the yield of Al_2O_3 increases with increasing $M_{\rm pr}$ and tends to be the same mass as Fe_3O_4, the mass fraction of Fe_3O_4 is limited to less than 0.1 for $M_{\rm pr} \geq 20\ M_\odot$, and that of Al_2O_3 is limited to less than 0.02 at most. In the mixed ejecta of PISNe (see Fig. 14*b*), SiO_2 is the most abundant grain, regardless of the progenitor mass. As in the mixed ejecta of CCSNe, around the low-mass end of the progenitor mass of PISNe, SiO_2 and Mg_2SiO_4 contribute to the total mass. As the progenitor mass increases, the masses of $MgSiO_3$ and Fe_3O_4 increase and approach almost the same mass, while the amount of Mg_2SiO_4 decreases. The total mass of dust grains is dominated by SiO_2, $MgSiO_3$, and Fe_3O_4, whose mass fractions are $\sim$0.7, 0.15, and 0.15, respectively.

5. SUMMARY

We investigate dust formation in the ejecta of Population III core-collapse and pair-instability supernovae, employing hydrodynamic models and the results of nucleosynthesis calculations by Umeda & Nomoto (2002). The time evolution of gas temperature in the ejecta is calculated by solving the radiative transfer equation together with the energy equation, taking into account the energy deposition from radioactive elements. Two extreme cases are considered for the elemental composition in the He-core: the unmixed case and the uniformly mixed case. In order to clarify what kind of grain species condenses in the ejecta, the formation of all possible condensates is calculated simultaneously by applying a theory of non–steady state nucleation and grain growth, under the assumption of complete formation of CO and SiO molecules. The results of the calculations are summarized as follows:

1. The species of newly formed dust grains are affected by the elemental composition in the ejecta. In the unmixed ejecta, a variety of grain species condense, corresponding to the elemental composition at the formation site: C and Si in the He layer; Al_2O_3, Mg_2SiO_4, and $MgSiO_3$ in the oxygen-rich layer (the O-Mg-Si and O-Si-Mg layers); MgO in the O-Mg-Si layer; SiO_2 in the O-Si-Mg layer; Si and FeS in the Si-S-Fe layer; and Fe in the Fe-Si-S layer. On the other hand, only oxide grains, such as Al_2O_3, Mg_2SiO_4, $MgSiO_3$, SiO_2, and Fe_3O_4, condense in the mixed ejecta. The main species of newly formed grains do not depend on the progenitor mass.

2. The average size of newly formed dust grains strongly depends on the concentration of the key species at the condensation time and at the formation site. In the unmixed ejecta, the range of average radius of each grain species spans a few orders of magnitude, depending on the grain species and the formation region. On the other hand, in the mixed ejecta, the average radius of each grain species is of almost the same order of magnitude in the entire region within the He core, reflecting the uniform elemental composition. The average radius of each grain species in both the unmixed and the mixed ejecta does not strongly depend on the progenitor mass and the explosion energy, but it is affected by the amount of ^{56}Ni in the ejecta. No dust grains condense with an average radius larger than 1 μm in the ejecta of Population III supernovae considered in this paper.

3. The size distribution function of a grain species condensed at a location in the ejecta is almost lognormal so long as the average radius is larger than 0.01 μm. The size distribution function summed up within the He core is lognormal for carbon, Fe, and SiO_2 grains condensed in the narrow, confined region of the unmixed ejecta; in the mixed ejecta, except for Al_2O_3 grains, the summed-up size distribution function is lognormal. The size distribution function summed up over all grain species is approximated by a power-law formula with an index of -3.5 for the larger radii and -2.5 for the smaller ones for both the unmixed and the mixed cases, being almost independent of the progenitor mass; the radius at the crossover point ranges from 0.004 to 0.1 μm, depending on the model of supernovae.

4. The total mass of newly formed dust grains increases with increasing progenitor mass and is generally much larger in the mixed case than in the unmixed case. The total mass of dust grains is 2%–5% of the progenitor mass for CCSNe with $13 M_\odot \leq M_{\rm pr} \leq 40\ M_\odot$ and 15%–30% of the progenitor mass for PISNe with $140 M_\odot \leq M_{\rm pr} \leq 260\ M_\odot$.[1] Thus, if PISNe populated the early universe, a large amount of dust would have been injected into the primordial interstellar medium.

5. The mass yield of each grain species depends on the progenitor mass. C, Fe, and Si are the major grain species in the unmixed ejecta of CCSNe with $M_{\rm pr} < 15\ M_\odot$. With increasing $M_{\rm pr}$, Si and Mg_2SiO_4 grains become dominant, and Mg_2SiO_4 grains are the most abundant for $M_{\rm pr} \geq 24\ M_\odot$. In the unmixed ejecta of PISNe, the most abundant grain is Mg_2SiO_4 for $M_{\rm pr} < 160\ M_\odot$; for $M_{\rm pr} \geq 160\ M_\odot$ the most abundant grain is Si, followed by Mg_2SiO_4, SiO_2, FeS, and Fe. In the mixed ejecta of CCSNe, SiO_2 and/or Mg_2SiO_4 are the major grain species contributing to the total mass. Being independent of the progenitor mass, in the mixed ejecta of PISNe, SiO_2 is the most abundant species, followed by Mg_2SiO_4 for $M_{\rm pr} < 160\ M_\odot$ and $MgSiO_3$ and Fe_3O_4 for $M_{\rm pr} \geq 170\ M_\odot$.

In the calculations, we treat only the formation of homogeneous grains, taking into account the chemical reactions at the condensation, but we do not consider the possibility of heterogeneous nucleation on the surface of precondensed grains. In fact, heterogeneous grains consisting of metal carbide cores and graphite mantles have been observed in

[1] After submitting this paper on 2003 June 28, we received a preprint from A. Ferrara, who obtained results basically similar to ours for the mass of the dust produced per PISN.

the Murchison meteorite (Bernatowicz et al. 1991, 1996). Also, we must consider the possibility of the formation of composite grains, such as Fe-Ni-Cr alloys, and thus whether the metal elements Ni, Co, and Cr, with relatively small abundances, can be locked into dust grains in the ejecta of supernovae. Also, as is discussed in Appendix B, it is very important to investigate the effect of the formation efficiency of CO and SiO molecules on the formation of dust grains, in order to clarify what kind of dust grains really condenses in the ejecta of supernovae. These subjects are left for future work.

Anyway, dust grains in the early universe play a critical role in the formation and evolution history of stars and galaxies. The investigation of the nature of dust grains in the early universe is essential, not only to investigating the evolution and structure of the early universe, but also to deducing the SFR and the IMF during the evolution of the universe from the relevant observations, because how much dust grains absorb stellar light and reemit it by thermal radiation depends on the chemical composition, size distribution, and amount of dust grains residing in interstellar space in galaxies and in the intergalactic medium. The evolution of dust grains is determined by the balance between their production in the ejecta of supernovae and their destruction by interstellar shock, as well as by the reverse shock penetrating into the ejecta. The efficiency of destruction by shock depends on the chemical composition and size of the dust grains. Therefore, the results of the calculations presented in this paper can be used as the basis to investigate the evolution of dust grains in the early universe.

The authors thank the anonymous referee for critical comments, which improved the manuscript. This work has been supported in part by a Grant-in-Aid for Scientific Research from the Japan Society for the Promotion of Sciences (13640229).

APPENDIX A

DUST FORMATION IN THE EJECTA OF HYPERNOVAE

HNe, with explosion energies larger than 10^{52} ergs, are proposed to reproduce the behavior of the observed early light curve of SN 1998bw (Iwamoto et al. 1998; Woosley, Eastman, & Schmidt 1999). Also, the analysis of the light curve of SN 1998bw (Nakamura et al. 2001) led to the conclusion that the mass of ^{56}Ni in the ejecta is 0.4 $M_\odot$, which is larger than the typical value of 0.07 $M_\odot$ in the ejecta of ordinary CCSNe. Furthermore, Umeda & Nomoto (2002) have claimed that primordial HNe well reproduce the observed elemental composition in metal-poor stars: [Zn/Fe] increasing with decreasing [Fe/H] for [Fe/H] ≤ -2.5 (Primas et al. 2000). In this appendix, we perform calculations of dust formation in the ejecta of Population III HNe to investigate the effect of explosion energy, as well as the amount of ^{56}Ni in the ejecta, on dust formation. We consider two models: one is H30A, with $M_{\rm pr} = 30\ M_\odot$, $E_{\rm exp} = 3 \times 10^{52}$ ergs, and $M(^{56}{\rm Ni}) = 0.07\ M_\odot$, and the other is H30B, for which $M_{\rm pr}$ and $E_{\rm exp}$ are the same as for H30A, but $M(^{56}{\rm Ni}) = 0.7\ M_\odot$.

Figure 15*a* shows the condensation time of each dust grain in the unmixed ejecta of H30A, with an explosion energy 30 times that of ordinary CCSNe but with $M(^{56}{\rm Ni})$ the same. The grain species formed in the ejecta and their condensation sequences are almost the same as in CCSNe and PISNe, except for Fe; the reason is that in this model, with an explosion energy of 3×10^{52} ergs, the innermost Fe-Si-S layer is not ejected, because of a shallow mass cut caused by adjusting $M(^{56}{\rm Ni})$ in the ejecta to 0.07 $M_\odot$. The condensation time of each grain species is about 200 days earlier than in CCSNe, because the gas temperature quickly decreases as a result of the high explosion velocity and low gas density in the ejecta. However, as can be seen from Figure 15*b*, the average radius of each dust grain formed in the ejecta is almost the same as that in the ejecta of CCSNe, because the early condensation time compensates for the decrease in gas density at the condensation time.

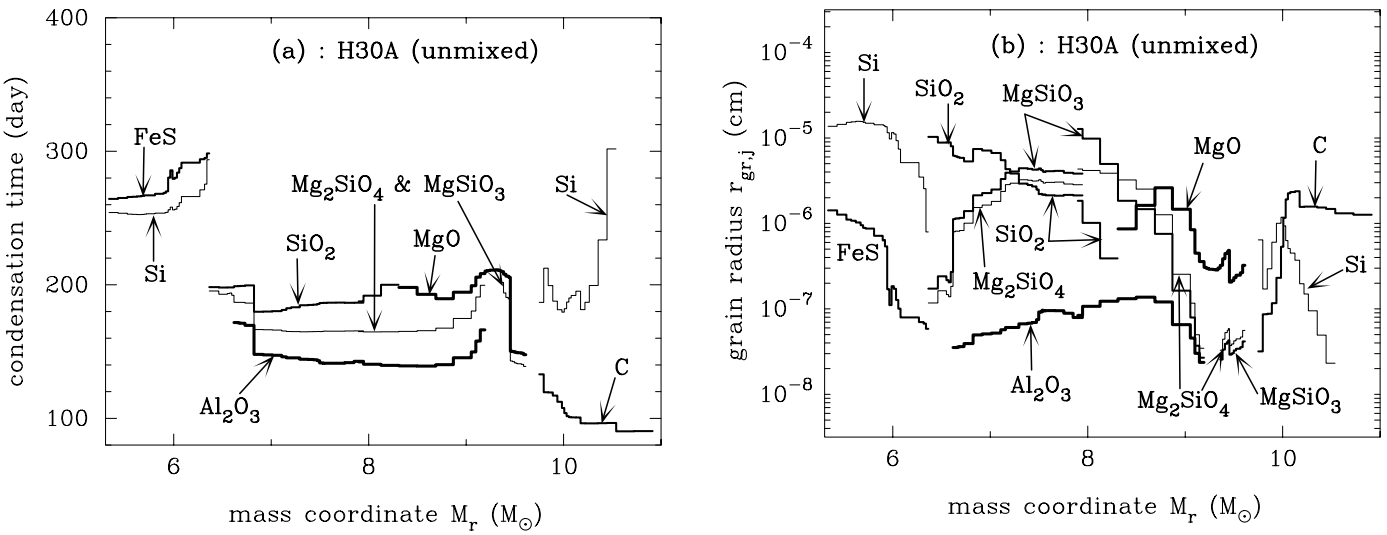

FIG. 15.—(*a*) Condensation times and (*b*) average radii of dust grains formed in the unmixed ejecta of H30A. [*See the electronic edition of the Journal for a color version of this figure.*]

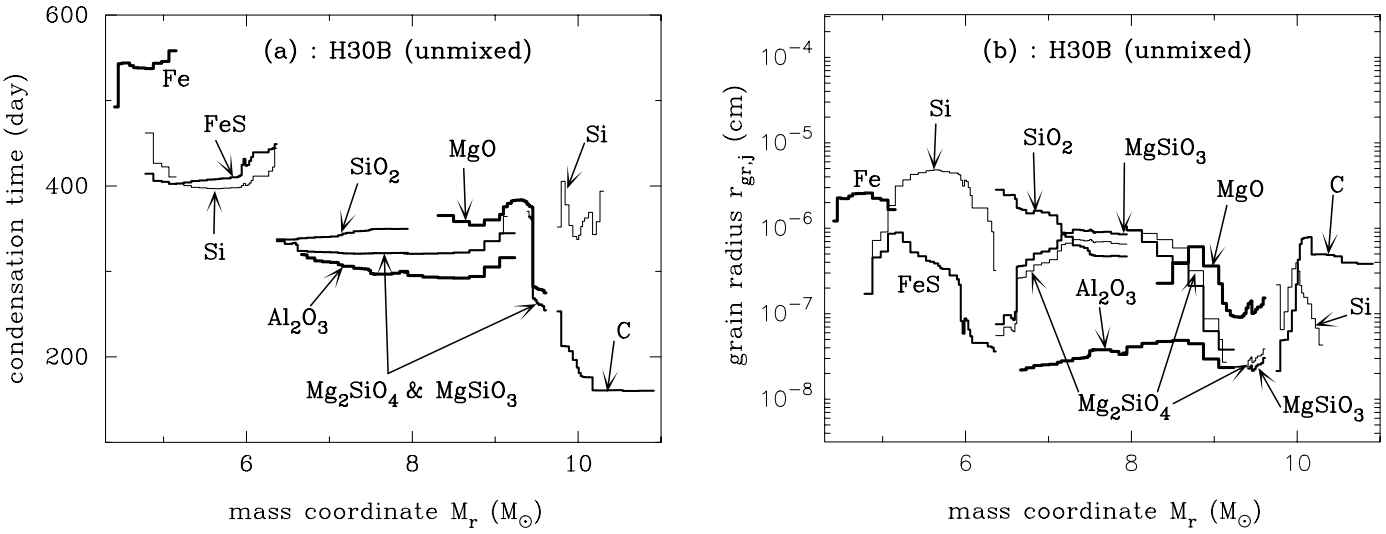

FIG. 16.—Same as Fig. 15, but for the unmixed ejecta of H30B. [*See the electronic edition of the Journal for a color version of this figure.*]

With $M(^{56}\mathrm{Ni}) = 0.7\ M_\odot$ and a higher gas temperature at a given time than in H30A, as is shown in Figure 16*a*, the condensation time of each grain species in the ejecta of H30B is about 150 days later than that of H30A. Therefore, the average radii of dust grains formed in the ejecta are a factor of 4–10 smaller than those in H30A (see Fig. 16*b*), depending on the concentration of the key species at the formation site. In contrast to the case in H30A, iron grains condense in the innermost Fe-Si-S layer, reflecting the deep mass cut at $M_r = 4.33\ M_\odot$.

From the results of the calculations, we can conclude here that the explosion energy, as well as the amount of ^{56}Ni in the ejecta, strongly affects the time evolution of the gas temperature. In the ejecta with a fixed amount of ^{56}Ni, a higher explosion energy results in an early condensation time, because the gas temperature quickly decreases as a result of the low gas density. However, the average radius of dust grains is not heavily affected, because the early condensation time compensates for the decrease in gas density at the formation site. On the other hand, the mass of ^{56}Ni in the ejecta strongly affects the average radius of dust grains formed in the ejecta with the same explosion energy. With increasing $M(^{56}\mathrm{Ni})$, the more delayed condensation time decreases the concentration of key species at the site of dust formation, which results in a smaller size of dust grains. Finally, it should be pointed out here that the amount of ^{56}Ni in the ejecta also affects the total mass of dust grains formed in the ejecta, as is depicted in Figure 13*a*; a large amount of ^{56}Ni in the ejecta with a deep mass cut for a fixed progenitor mass results in a large mass in the ejecta, as well as a large total mass of dust grains, and vice versa.

APPENDIX B

THE EFFECT OF THE FORMATION EFFICIENCY OF CO AND SiO MOLECULES ON DUST FORMATION

In the calculations of dust formation, we assumed the complete formation of CO and SiO molecules. Formation of CO and SiO molecules prior to dust formation was observed in SN 1987A (e.g., Bouchet & Danziger 1993). Furthermore, recent observations have suggested that the formation of CO molecules is a common phenomenon in the ejecta of CCSNe (e.g., Gerardy et al. 2002). Formation of CO and SiO molecules is usually considered to be complete and controls the chemistry in the astrophysical environments of interest to dust formation, such as in the circumstellar envelopes of AGB stars. However, in the ejecta of supernovae, these molecules are destroyed by collisions with high-energy electrons, as well as with ionized inert gaseous atoms produced by the decay of radioactive elements, and the abundance of these molecules is determined by the balance between formation and destruction (Liu & Dalgarno 1994, 1996). Thus, in the ejecta of supernovae, for example, it is expected that free carbon atoms are available for the formation of carbon-bearing dust grains even in the ejecta of $\mathrm{C/O} < 1$. This aspect has been extensively pursued by Clayton et al. (1999, 2001) in investigating the origin of presolar grains identified as SUNOCONs. The abundances of CO and SiO molecules depend on the abundance of free electrons, as well as ionized inert gas. Thus, in this appendix, to simplify the calculations, we investigate the effect of the formation efficiency of CO and SiO molecules on dust formation, by referring to the formation efficiency of CO and SiO molecules observed in SN 1987A as a template and introducing the parameters f_{C} and f_{Si}, which represent the mass fractions of C and Si atoms not locked into CO and SiO molecules, respectively.

In the ejecta of SN 1987A, the masses of CO and SiO molecules have been evaluated to be $(3\text{–}6) \times 10^{-3}$ and $(0.4\text{–}1) \times 10^{-3}$ $M_\odot$, respectively, during 300–600 days after the explosion (Liu & Dalgarno 1994, 1995), which correspond to $f_{\mathrm{C}} \simeq 0.99$ and $f_{\mathrm{Si}} \simeq 0.9$ in the oxygen-rich core, respectively. The mass fractions $f_{\mathrm{C}} = 0.99$ and $f_{\mathrm{Si}} = 0.9$ being fixed, Figures 17*a* and 17*b* show the mass of newly formed grain species versus f_{Si} and f_{C}, respectively, at the location of $M_r = 3.5\ M_\odot$ in the O-Mg-Si layer of C20. In the calculations, we consider the SiO molecule the key species for the formation of Mg silicate grains. Of course, the formation of Al_2O_3 grains is not affected by the formation efficiency of these molecules. The mass of C and Si grains

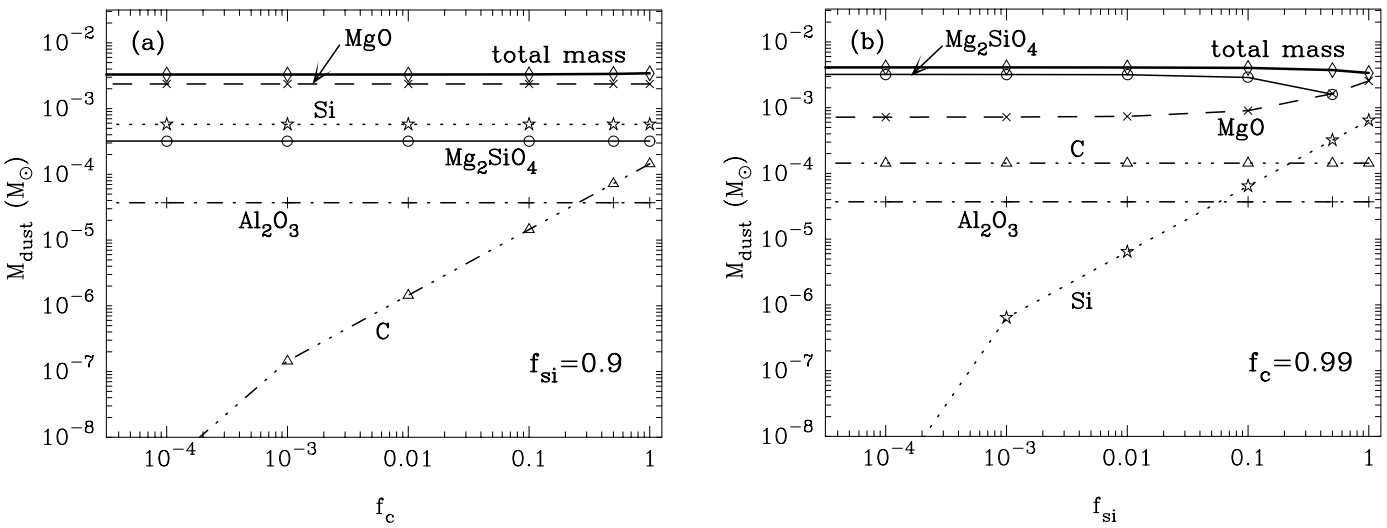

FIG. 17.—Mass of each grain species vs. mass fractions of carbon f_C and silicon f_{Si} not locked into CO and SiO molecules, at $M_r = 3.5\ M_\odot$ in the O-Mg-Si layer of the unmixed ejecta of C20. (*a*) Mass vs. f_C when f_{Si} is fixed to 0.9. (*b*) Mass vs. f_{Si} when f_C is fixed at 0.99. [*See the electronic edition of the Journal for a color version of this figure.*]

increases with increasing f. As can be seen from Figure 17*a*, except for the formation of carbon grains, the formation efficiency of CO molecules does not influence the formation of other grain species. Also, the formation of carbon grains does not affect the total mass of dust grains at this location, since O and Mg atoms are much more abundant than C atoms (see Fig. 1*a*). The average size of carbon grains increases with increasing f_C but is limited to less than 0.04 μm, even at $f_C = 1$. On the other hand, the formation efficiency of SiO molecules strongly affects the mass abundance of Si- and/or Mg-bearing grains; with increasing f_{Si}, the decrease of SiO molecules not only results in the formation of Si grains, but also increases the mass of MgO grains with the reduction of the mass of Mg_2SiO_4 grains, which is prominent for $f_{Si} \geq 0.1$. The average radii of Si and MgO grains increase and reach $\sim$0.1 μm with increasing f_{Si}; the average radius of Mg_2SiO_4 grain decreases. At this location, the formation efficiency of CO and SiO molecules does not affect the total mass of dust grains, because the abundance of C atoms is 2 orders of magnitude lower than that of O atoms. However, if $f_C = 0.99$ in the outer region of the O-Mg-Si layer ($4\ M_\odot \leq M_r \leq 5\ M_\odot$ for C20), many more carbon dust grains could condense, and the average radius could reach to from $\sim$0.4 to $\sim$1 μm, depending on the abundance of carbon atoms at the formation site.

Finally, it should be addressed here that we cannot realize the formation of SiC grains with radii comparable to those of presolar SiC grains identified as SUNOCONs by changing the parameters f_C and f_{Si}. The formation of SiC grains competes with the formation of carbon and silicon grains; carbon atoms available for formation of SiC grains are locked into carbon grains prior to the formation of SiC grains, and the same is true for silicon atoms. This implies that the amount and size are very small even if SiC grains condense. Therefore, as proposed by Deneault et al. (2003), special conditions and/or chemical pathways might have to be considered in order to realize the formation of SiC grains identified as SUNOCONs.

Anyway, the results of the calculations show that the reduction of the formation efficiency of CO and SiO molecules leads to the formation of C and Si grains. Furthermore, the formation efficiency of SiO molecules affects the abundance and size of Si- and/or Mg-bearing grains. However, we must keep in mind that in the calculations the stability of C and Si grains is not taken into account; in the environment with a lot of free oxygen atoms, C and Si grains could be easily oxidized if their sizes were small, though Clayton et al. (2001) have claimed that carbon grains are stable against the oxidation in the oxygen-rich environment. Oxidation of Si grains produces SiO_2 grains and/or evaporates SiO molecules available for formation of Mg silicate grains, and it may be possible that another chemical pathway leads to the formation of Mg silicate grains without SiO molecules, resulting in more oxide grains even if the formation efficiency is very low. These aspects should be pursued to clarify how much dust, as well as what kind of oxide grains, really forms in the ejecta of supernovae.

REFERENCES

Amari, S., & Zinner, E. 1997, in AIP Conf. Proc. 402, Astrophysical Implications of the Laboratory Study of Presolar Materials, ed. T. J. Bernatowicz & E. Zinner (Woodbury: AIP), 287
Arendt, R. G., Dwek, E., & Moseley, S. H. 1999, ApJ, 521, 234
Arnett, W. D., Bahcall, J. N., Kirshner, R. P., & Woosley, S. E. 1989, ARA&A, 27, 629
Bernatowicz, T. J., Amari, S., Zinner, E. K., & Lewis, R. S. 1991, ApJ, 373, L73
Bernatowicz, T. J., Cowsik, R., Gibbons, P. C., Lodders, K., Fegley, B., Jr., Amari, S., & Lewis, R. S. 1996, ApJ, 472, 760
Boni, R. E., & Derge, D. 1956, J. Metals, 8, 53
Bouchet, P., & Danziger, I. J. 1993, A&A, 273, 451
Bromm, V., Coppi, P. S., & Larson, R. B. 2002, ApJ, 564, 23
Chase, M. W., Jr., Davies, C. A., Downey, J. R., Jr., Frurip, D. J., McDonald, R. A., & Syverud, A. N. 1985, JANAF Thermochemical Tables, 3d ed. J. Phys. Chem. Ref. Data, 14, Suppl. 1
Chigai, T., Yamamoto, T., & Kozasa, T. 1999, ApJ, 510, 999
Christlieb, N., et al. 2002, Nature, 419, 904
Clayton, D. D., Deneault, E. A.-N., & Meyer, B. S. 2001, ApJ, 562, 480
Clayton, D. D., Liu, W., & Dalgarno, A. 1999, Science, 283, 1290
Colgan, S. W. J., Haas, M. R., Erickson, E. F., Lord, S. D., & Hollenbach, D. J. 1994, ApJ, 427, 874
Deneault, E. A.-N., Clayton, D. D., & Heger, A. 2003, ApJ, 594, 312

Dotani, T., Hayashida, K., Inoue, H., Itoh, M., & Koyama, K. 1987, Nature, 330, 230
Douvion, T., Lagage, P. O., Cesarsky, C. J., & Dwek, E. 2001a, A&A, 373, 281
Douvion, T., Lagage, P. O., & Pantin, E. 2001b, A&A, 369, 589
Drake, R. P., et al. 2002, ApJ, 564, 896
Dunne, L., Eales, S., Ivison, R., Morgan, H., & Edmunds, M. 2003, Nature, 424, 285
Dwek, E. 1998, ApJ, 501, 643
Dwek, E., Dinerstein, H. L., Gillett, F. C., Hauser, M. G., & Rice, W. L. 1987, ApJ, 315, 571
Elliott, J. F., & Gleiser, M. 1960, Thermochemistry for Steelmaking, Vol. 1 (Reading: Addison-Wesley)
Elliott, J. F., Gleiser, M., & Ramakrishna, V. 1963, Thermochemistry for Steelmaking, Vol. 2 (Reading: Addison-Wesley)
Elmhamdi, A., et al. 2003, MNRAS, 338, 939
Fesen, R. A., & Blair, W. P. 1990, ApJ, 351, L45
Gail, H.-P., Keller, R., & Sedlmayr, E. 1984, A&A, 133, 320
Gerardy, C. L., Fesen, R. A., Nomoto, K., Maeda, K., Höflich, P., & Wheeler, J. C. 2002, PASJ, 54, 905
Hachisu, I., Matsuda, T., Nomoto, K., & Shigeyama, T. 1990, ApJ, 358, L57
Hasegawa, H., & Kozasa, T. 1988, Prog. Theor. Phys. Suppl., 96, 107
Hauser, M. G., & Dwek, E. 2001, ARA&A, 39, 249
Heger, A., & Woosley, S. E. 2002, ApJ, 567, 532
Hester, J. J., Graham, J. R., Beichman, C. A., & Gautier, T. N., III 1990, ApJ, 357, 539
Hirashita, H., & Ferrara, A. 2002, MNRAS, 337, 921
Hirashita, H., Hunt, L. K., & Ferrara, A. 2002, MNRAS, 330, L19
Itoh, M., Kumagai, S., Shigeyama, T., Nomoto, K., & Nishimura, J. 1987, Nature, 330, 233
Iwamoto, K., et al. 1998, Nature, 395, 672
———. 2000, ApJ, 534, 660
Kozasa, T., Dorschner, J., Henning, T., & Stognienko, R. 1996, A&A, 307, 551
Kozasa, T., & Hasegawa, H. 1987, Prog. Theor. Phys, 77, 1402
———. 1988, Icarus, 73, 180
Kozasa, T., Hasegawa, H., & Nomoto, K. 1989a, ApJ, 344, 325
———. 1989b, ApJ, 346, L81
———. 1991, A&A, 249, 474
Kumagai, S., Itoh, M., Shigeyama, T., Nomoto, K., & Nishimura, J. 1988, A&A, 197, L7
Lagage, P. O., Claret, A., Ballet, J., Boulanger, F., Cesarsky, C. J., Cesarsky, D., Fransson, C., & Pollock, A. 1996, A&A, 315, L273
Liu, W., & Dalgarno, A. 1994, ApJ, 428, 769
———. 1995, ApJ, 454, 472
———. 1996, ApJ, 471, 480
Loeb, A., & Haiman, Z. 1997, ApJ, 490, 571
Lucy, L. B., Danziger, I. J., Gouiffes, C., & Bouchet, P. 1989, in IAU Colloq. 120, Structure and Dynamics of the Interstellar Medium, ed. G. Tenorio-Tagle, M. Moles, & J. Melnick (LNP 350; Berlin: Springer), 164
Mathis, J. S., Rumpl, W., & Nordsieck, K. H. 1977, ApJ, 217, 425
Meikle, W. P. S., Spyromilio, J., Allen, D. A., Varani, G.-F., & Cumming, R. J. 1993, MNRAS, 261, 535
Mezger, P. G., Tuffs, R. J., Chini, R., Kreysa, E., & Gemünd, H.-P. 1986, A&A, 167, 145
Nakamura, F., & Umemura, M. 2001, ApJ, 548, 19
Nakamura, T., Mazzali, P. A., Nomoto, K., & Iwamoto, K. 2001, ApJ, 550, 991
Nomoto, K., Maeda, K., Mazzali, P. A., Umeda, H., Deng, J., & Iwamoto, K. 2003, in Stellar Collapse, ed. C. L. Fryer (Dordrecht: Kluwer), in press (astro-ph/0308136)
Nomoto, K., Mazzali, P. A., Nakamura, T., Iwamoto, K., Danziger, I. J., & Patat, F. 2001, in Supernovae and Gamma-Ray Bursts, ed. M. Livio, N. Panagia, & K. Sahu (Cambridge: Cambridge Univ. Press), 144
Overbury, S. H., Bertrand, P. A., & Somorjai, G. A. 1975, Chem. Rev., 75, 547
Pei, Y. C., & Fall, S. M. 1995, ApJ, 454, 69
Pettini, M., King, D. L., Smith, L. J., & Hunstead, R. W. 1997, ApJ, 478, 536
Pettini, M., Smith, L. J., Hunstead, R. W., & King, D. L. 1994, ApJ, 426, 79
Primas, F., Brugamyer, E., Sneden, C., King, J. R., Beers, T. C., Boesgaard, A. M., & Deliyannis, C. P. 2000, in The First Stars, ed. A. Weiss, T. G. Abel, & V. Hill (Berlin: Springer), 51
Rhee, S. K. 1970, J. Am. Ceram. Soc., 53, 639
Robie, R. A., & Waldbaum, D. R. 1968, Thermodynamic Properties of Minerals and Related Substances at 298.15 Degrees K and One Atmosphere Pressure and at Higher Temperatures (USGS Bull. B 1259; Reston: USGS)
Schneider, R., Ferrara, A., & Salvaterra, R. 2003a, MNRAS, submitted (astro-ph/0307087)
Schneider, R., Ferrara, A., Salvaterra, R., Omukai, K., & Bromm, V. 2003b, Nature, 422, 869
Shigeyama, T., & Nomoto, K. 1990, ApJ, 360, 242
Tabak, R. G., Hirth, J. P., Meyrick, G., & Roark, T. P. 1975, ApJ, 196, 457
Todini, P., & Ferrara, A. 2001, MNRAS, 325, 726
Travaglio, C., Gallino, R., Amari, S., Zinner, E., Woosley, S., & Lewis, R. S. 1999, ApJ, 510, 325
Umeda, H., & Nomoto, K. 2002, ApJ, 565, 385
———. 2003a, Nature, 422, 871
———. 2003b, ApJ, submitted (astro-ph/0308029)
Whitelock, P. A., et al. 1989, MNRAS, 240, 7P
Wooden, D. H., Rank, D. M., Bregman, J. D., Witteborn, F. C., Tielens, A. G. G. M., Cohen, M., Pinto, P. A., & Axelrod, T. S. 1993, ApJS, 88, 477
Woosley, S. E., Eastman, R. G., & Schmidt, B. P. 1999, ApJ, 516, 788
Woosley, S. E., & Weaver, T. A. 1995, ApJS, 101, 181
Yamamoto, T., Chigai, T., Watanabe, S., & Kozasa, T. 2001, A&A, 380, 373
Zinner, E. 1998, Meteoritics Planet. Sci., 33, 549